was extended to generate retinal photoreceptor cells. SFEB/DL-treated differentiated cells were incubated in the RA/T medium [13] [G-MEM containing 5% KSR, N2 supplement (GIBCO), retinoic acid (1 μM, Sigma), taurine (100 μM, Sigma), 0.1 mM nonessential amino acids, 1 mM sodium pyruvate, 0.1 mM 2-mercaptoethanol, 50 units/ml penicillin, and 50 μg/ml streptomycin].

For directed differentiation, human iPS colonies were partially dissociated into clumps (5–10 cells/clump) by treatment with 0.25% trypsin and 0.1 mg/ml collagenase IV in PBS containing 1 mM $CaCl_2$ and 20% KSR, followed by gentle trituration. Feeders were removed by incubation of the iPS clumps on a gelatin-coated dish. Human iPS clumps, at a density of 6.7×10^2 clumps/ml, were incubated in a 100 mm low cell binding dish in human ES medium for 2 days, in 20% KSR-containing ES differentiation medium (G-MEM, 0.1 mM nonessential amino acids, 1 mM pyruvate and 0.1 mM 2-mercaptoethanol) for 4 days, then in 15% KSR-containing ES differentiation medium for 8 days, and subsequently in 10% KSR-containing ES differentiation medium for 6 days. Dkk-1 (100 ng/ml) and Lefty A (500 ng/ml) were applied to the medium for 20 days while in suspension culture. Human iPS cell aggregates were then replated en bloc on poly-D-lysine/laminin/fibronectin-coated 8-well culture slides at a density of 10–15 aggregates/cm^2. In adherent

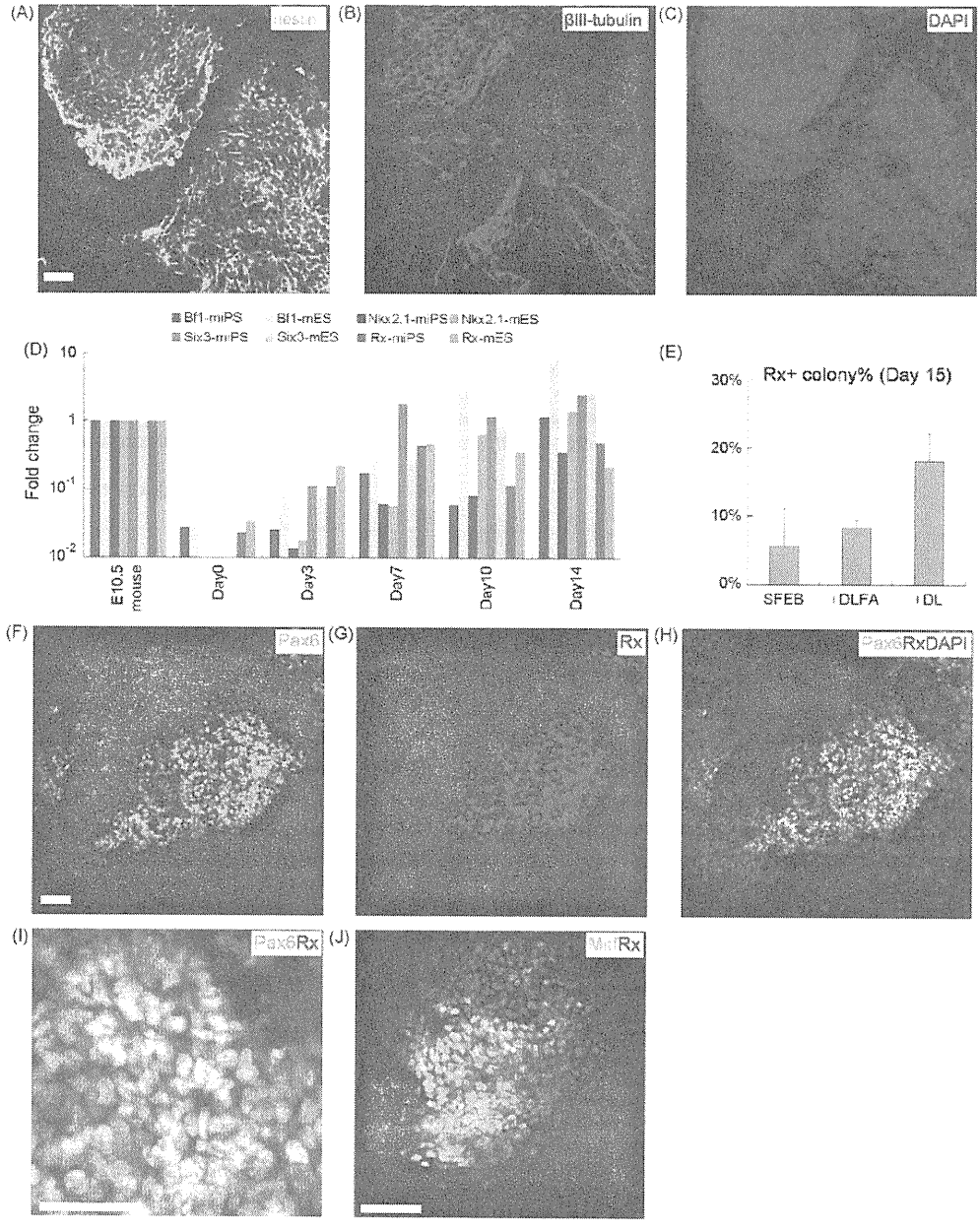

Fig. 1. Directed differentiation of neural and retinal progenitors from mouse induced pluripotent stem (iPS) cells. (A–C) Immunostaining of mouse iPSCs in SFEB conditions with anti-nestin and anti-βIII-tubulin antibodies on day 9. Cell nuclei were counterstained with 4′,6-diamidino-2-phenylindole (DAPI). (D) Fold change of the gene expression by real-time RT-PCR analysis of the neural markers *Bf1* and *Nkx2.1*, the eye field marker *Six3* and the retinal progenitor marker *Rx* in mouse iPSCs under SFEB culture conditions (reference; head portion of mouse embryo [E10.5]). (E) The percentage of $Rx^+/Pax6^+$ colonies in different culture conditions of mouse iPSCs on day 15. SFEB: a serum-free, feeder-free suspension culture. SFEB/DLFA: the SFEB culture combined with Dkk-1 (100 ng/ml) and the Lefty A (500 ng/ml) on day 0, FBS (5%) on day 4, and Activin A (100 ng/ml) on day 5. SFEB/DL: the SFEB culture combined with Dkk-1 (100 ng/ml) and the Lefty A (500 ng/ml) from day 0 to 9. (F–H) Immunostaining of mouse iPSCs in SFEB/DL conditions with anti-Rx and anti-Pax6 antibodies on day 15. (I) Magnified view of $Rx^+/Pax6^+$ cells in mouse iPSCs under SFEB/DL conditions on day 15. (J) Immunostaining of mouse iPSCs in SFEB/DL conditions with anti-Mitf and anti-Rx antibodies on day 15. Scale bars: 50 μm.

cultures, cells were incubated in 10% KSR-containing ES differentiation medium. For photoreceptor differentiation, human iPSCs were incubated under SFEB/DL conditions for 90 days, and subsequently in RA/T medium for at least 30 days. The medium was changed every day.

Total RNA was extracted from cultured iPSCs with TRIzol reagent (Invitrogen). Complementary DNA was then synthesized from RNA with a first-strand cDNA synthesis kit (GE Healthcare Bio-Sciences, Piscataway, NJ). The synthesized cDNA from each sample was amplified with Power SYBR Green PCR Master Mix (Applied Biosystems, Foster City, CA) using gene-specific primers in a step cycle program for 40 cycles under the following conditions: denaturation at 95 °C for 15 s, annealing at 60 °C for 60 s. Primers used for RT-PCR analyses were listed in supplementary methods. Data normalization was performed in reference to the gene expression level of the head portion of mouse E10.5 embryo in neural and retinal progenitor marker genes (*Bf1*, *Nkx2.1*, *Six3*, *Rx*), undifferentiated iPSCs in undifferentiated cell marker genes (*Oct3/4*, *Nanog*) or the neonatal mouse retina in photoreceptor marker genes (*Crx*).

Immunocytochemistry was performed as described previously [13]. Briefly, cultured iPSCs were fixed with 4% paraformaldehyde for 15 min at 25 °C, washed with phosphate buffered saline (PBS) and blocked with 5% goat serum and 0.3% Triton X-100 (Sigma) in PBS. The samples were incubated overnight at 4 °C with primary antibodies and 0.3% Triton X-100. After primary antibodies were removed and the samples were washed, secondary antibodies were applied for 1 h at 25 °C. Primary and secondary antibodies were listed in supplementary methods. Cell nuclei were counterstained with 4′,6-diamidino-2-phenylindole (DAPI; 1 μg/ml, molecular probes—Invitrogen). Labeled cells were imaged with a confocal laser scanning microscope (Radiance 2100; Bio-Rad Laboratories, Hercules, CA).

Undifferentiated and SFEB/DL-treated iPS cell aggregates were dissociated as previously described [6]. The aggregates were suspended with 0.25% trypsin/EDTA (Invitrogen) and DNase I (10 μg/ml, Sigma) into single cells. After neutralization of trypsin with DMEM containing 10% FBS, the cells were resuspended in HBSS containing 0.1% BSA and 5 μg/ml propidium iodide (Sigma), and passed through a cell strainer (BD, Franklin Lakes, NJ). Cells were counted by FACS Aria (BD Biosciences), and the data were analyzed with FACS Diva software (BD Biosciences). Dead cells were excluded by gating forward and side scatter as well as by PI staining.

Data are expressed as means ± S.E.M. The reproducibility of the results was confirmed in at least three independent sets of experiments. The statistical significance of difference was evaluated with an unpaired *t*-test or with one-way analysis of variance (ANOVA) followed by Dunnett's test. Probability values less than 5% were considered significant.

A published study has reported that mouse ES cells can be efficiently differentiated into neural progenitors in a serum-free, feeder-free suspension culture (SFEB) [18]. In addition, retinal progenitors can be induced by combining soluble factors with the SFEB method [6,13]. To induce differentiation of mouse iPSCs with the SFEB method, mouse iPSCs (iPS-MEF-Ng-20D-17) [12] were seeded in Petri dishes as suspension cultures. After 6 days of floating culture, the aggregates were adhered onto glass slides coated with poly-D-lysine, laminin, and fibronectin, and cultured for another 3 days (day 9). Immunocytochemical analysis revealed that nearly all of the aggregates expressed nestin (99.3 ± 0.65% of total colonies) and βIII-tubulin (98.0 ± 1.1% of total colonies) (Fig. 1A–C). Since Wnt and TGFβ signals have negative effects on mammalian neural differentiation [1,14], we applied the Wnt antagonist Dkk-1 (100 ng/ml) and the Nodal antagonist Lefty A (500 ng/ml) during suspension culture (SFEB/DL method) [18]. According to the method which was previously reported with mouse ES cells [6], fetal bovine serum (FBS; Invitrogen) was added in the medium with 5% at the final concentration on day 4, and Activin A (100 ng/ml; R&D) was added in the medium on day 5 (SFEB/DLFA method). Floating aggregates were plated on coated slides. Cells were fixed on day 9 and used for subsequent immunocytochemical analysis. However, we could not detect cells positive for the retinal progenitor markers Rx, Pax6 and Mitf. We then prolonged the duration of adhesion culture period and examined the mRNA expression of central nervous system (CNS) region-specific markers by real-time PCR. The expression of telencephalic markers *Bf1*, *Nkx2.1* and *Six3* and the eye field marker *Rx* in iPSCs were found to be increased after inducing differentiation by the SFEB/DL method. This observation is similar to the differentiation of ES cells (Fig. 1D). Mouse iPSCs were cultured under the SFEB conditions and probed for the retinal progenitor markers Rx, Pax6 and Mitf. On day 15, we observed 18.1 ± 4.1% of total colonies double positive for both Rx and Pax6 under the SFEB/DL conditions (5.56 ± 5.6% under the SFEB conditions and 8.26 ± 1.2% under the SFEB/DLFA conditions) (Fig. 1E–I). The SFEB/DL method tends to increase the number of Rx^+ cells than the SFEB method, although there was no statistical significant difference between them. Under SFEB/DL conditions, 22.3 ± 3.9% of cells was Rx^+ within the positive colonies. In addition, 36.2 ± 5.1% of total colonies cultured under SFEB/DL conditions also expressed Mitf, a marker of RPE progenitors (11.4 ± 3.4% of cells in those colonies; Fig. 1J). The $Mitf^+$cells and Rx^+cells were frequently found in the same clusters. We conclude from these results that mouse iPSCs differentiate into retinal progenitors following SFEB/DL-treatment.

Second, we assessed the number of undifferentiated cells during differentiation. Mouse Nanog-iPS cells express GFP protein with Nanog [12]. Under conditions that did not induce differentiation, 96.2 ± 0.10% of total cells was positive for Nanog-GFP by flow cytometry (Fig. 2A). In contrast, the level of fluorescence of Nanog-GFP significantly decreased in iPSCs as the SFEB or SFEB/DL culture progressed. At day 8 and day 15, 4.05 ± 0.62% and 0.60 ± 0.04% of cells were Nanog-GFP^+, respectively (Fig. 2B and C). Thus, a small number of cells remained undifferentiated even after 15 days. Real-time PCR analysis also revealed that expression of markers for undifferentiated cells Oct3/4 and Nanog gradually decreased over the period of differentiation (Fig. 2D). This finding parallels our observation with mouse ES cells cultured under identical conditions (data not shown).

Third, we examined the differentiation potential of retinal progenitors derived from mouse iPSCs. RPE cells form tight junctions

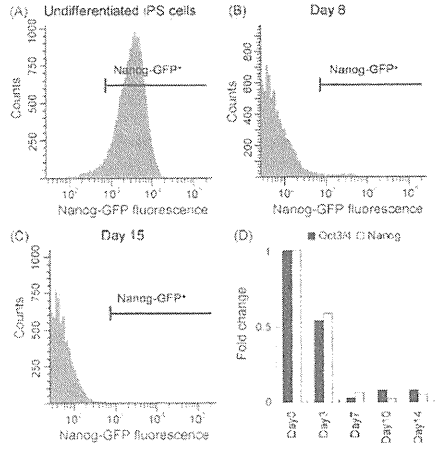

Fig. 2. The analysis of residual undifferentiated mouse iPSCs under SFEB/DL conditions. (A–C) The number of residual undifferentiated iPSCs present after differentiation was determined by flow cytometry of Nanog-GFP positive undifferentiated iPSCs on days 8 and 15 under SFEB/DL conditions. (D) Fold change of the gene expression by RT-PCR analysis of the undifferentiated cell markers *Oct3/4* and *Nanog* in mouse iPSCs under SFEB/DL conditions (reference: undifferentiated mouse iPSCs).

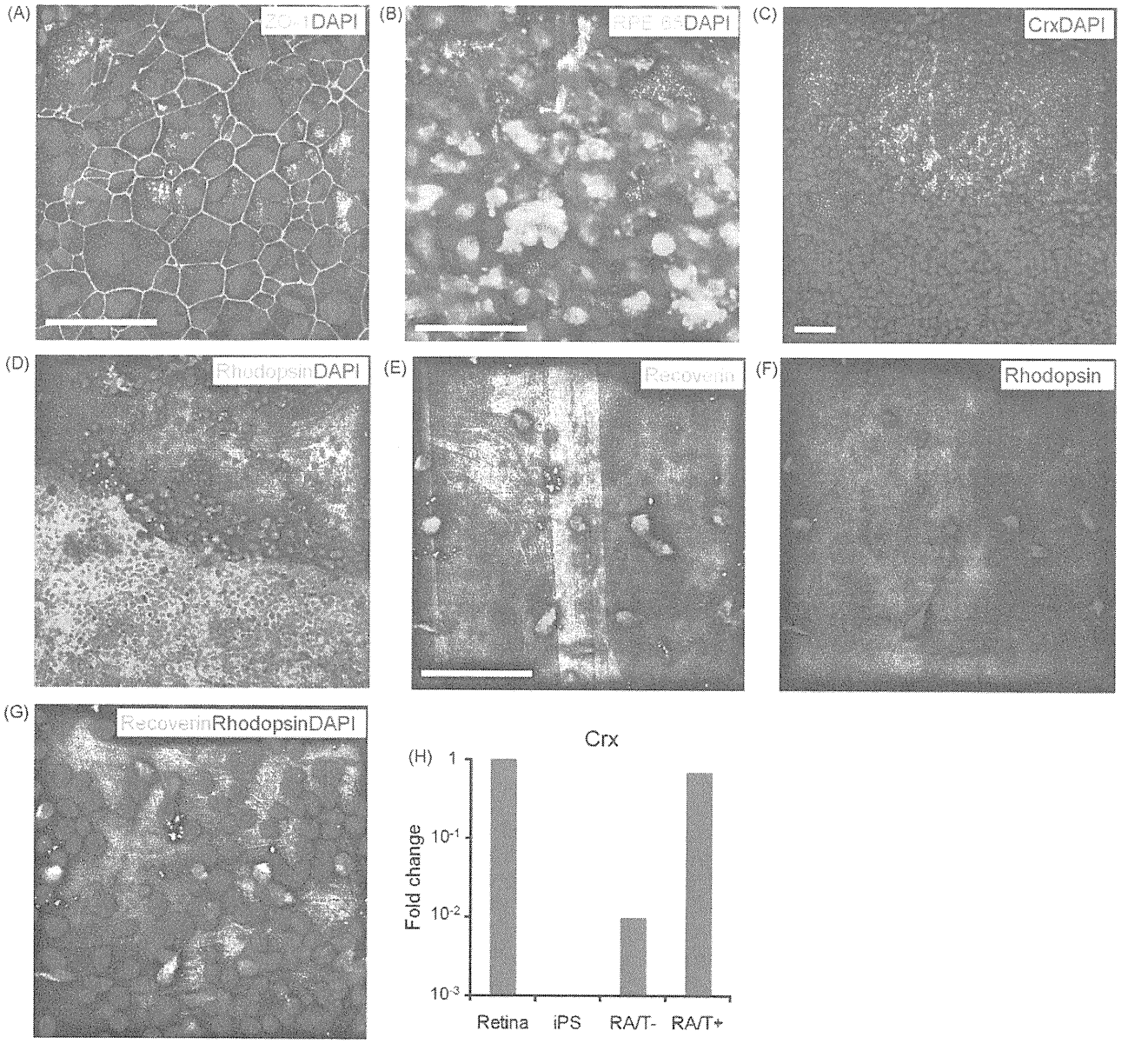

Fig. 3. Differentiation of mouse iPSCs into putative retinal pigment epithelium and photoreceptors. (A) Staining of tight junctions with an anti-ZO-1 antibody in mouse iPSCs under SFEB/DL conditions on day 30. (B) Immunostaining of mouse iPSCs with anti-RPE65 antibodies on day 45 in SFEB/DL conditions. (C and D) Immunostaining of mouse iPSCs with anti-Crx and anti-rhodopsin antibodies on day 45 in SFEB/DL conditions following the application of retinoic acid (1 μM) and taurine (100 μM). (E–G) Immunostaining of mouse iPSCs with anti-recoverin and anti-rhodopsin antibodies on day 45 in SFEB/DL conditions following the application of retinoic acid (1 μM) and taurine (100 μM). (H) Fold change of the gene expression by RT-PCR analysis of the photoreceptor marker *Crx* in mouse iPSCs under SFEB/DL conditions with or without retinoic acid and taurine treatment on day 45 (reference; neonatal mouse retina). Scale bars: 50 μm.

with hexagonal morphology *in vivo*. Therefore, we determined the expression of ZO-1, a tight junction marker. On day 30, ZO-1 was expressed at the lateral border of polygonal-shaped cells cultured under SFEB/DL culture conditions (Fig. 3A). We also found cells positive for a RPE specific marker, RPE-65 on day 45 (Fig. 3B). Next, according to the differentiation method for ES cells [13], we treated mouse iPSCs differentiated with the SFEB/DL method with retinoic acid (1 μM) and taurine (100 μM), both of which are important for photoreceptor genesis [8], beginning at differentiation day 24 (RA/T treatment). On day 45, we observed cells that were immunopositive for both the photoreceptor precursor marker Crx and the mature rod photoreceptor marker rhodopsin (Fig. 3C and D). The rhodopsin$^+$ cells co-expressed another photoreceptor marker, recoverin (Fig. 3E–G). Real-time PCR analysis showed fold increase of Crx expression in differentiated mouse iPSCs with RA/T treatment than in those without RA/T treatment (Fig. 3H). Thus, we conclude that induced retinal progenitors have competence to differentiate into putative photoreceptors and RPE cells.

Finally, we examined whether human iPSCs could differentiate into retinal progenitors when treated with a method similar to that used for human ES cells. Human iPSCs (201B6, 201B7 and 253G1) [16,10] were dissociated into small clumps of 5–10 cells and seeded in Petri dishes as suspension cultures with serum-free medium containing Dkk-1 (100 ng/ml) and Lefty A (500 ng/ml). Under these conditions, human iPSCs formed embryoid body-like aggregates. On day 20, aggregates were plated onto glass slides coated with poly-D-lysine, laminin, and fibronectin. On day 35, we observed marked expression of the neural differentiation marker nestin and

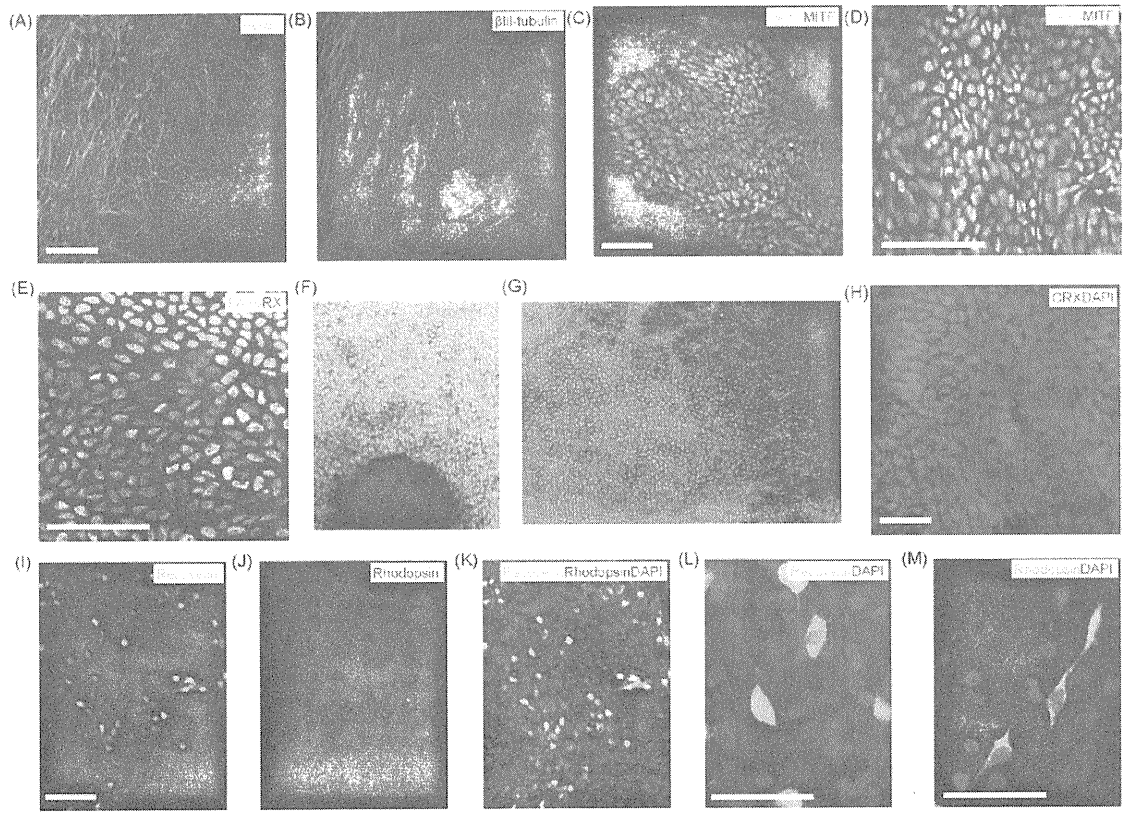

Fig. 4. Directed differentiation of neural and retinal progenitors and induction of photoreceptor properties from human induced pluripotent stem (iPS) cells. (A and B) Immunostaining of human iPSCs in SFEB/DL conditions with anti-nestin and anti-βIII-tubulin antibodies on day 35. (C and D) Presumptive RPE cells immunopositive for anti-Mitf and anti-Pax6 antibodies in human iPS cell cultures in SFEB/DL conditions on day 35. (E) Retinal progenitor cells immunopositive for anti-Rx and anti-Pax6 antibodies in human iPS cell cultures in SFEB/DL conditions on day 35. (F and G) Pigmented cells in human iPS cell cultures in SFEB/DL conditions display RPE-like polygonal morphologies on day 60. (H) Immunostaining of human iPSCs in SFEB/DL conditions with anti-Crx antibody on day 80. (I–M) Immunostaining of human iPSCs with anti-recoverin and anti-rhodopsin antibodies on day 120 in SFEB/DL conditions following the application of retinoic acid (1 μM) and taurine (100 μM). Scale bars: 50 μm.

βIII-tubulin (Fig. 4A and B). Under SFEB/DL conditions, 29.8 ± 4.0% of total colonies of these differentiated iPSCs were $MITF^+/PAX6^+$ (Fig. 4C and D) and 19.4 ± 4.9% were $RX^+/PAX6^+$ (Fig. 4E). These results mirror our results with human ES cells [13]. The $MITF^+$ cells were frequently found in close proximity to RX^+ cells. Thus, human iPSCs can be differentiated into retinal progenitors. On day 40, pigmented cells were evident under the light microscopy in the SFEB/DL cultures (38.8 ± 6.8% of total colonies). We could observe these differentiated cells in two human iPS cell lines 201B7 and 253G1; however, pigmented cells, $MITF^+/PAX6^+$ or $RX^+/PAX6^+$ cells were not detected in an iPS cell line 201B6 with the same differentiation method. We then used the cell lines 201B7 and 253G1 for further analyses. Over time, these cells adopted a polygonal morphology, a characteristic of RPE cells (Fig. 4F and G). On day 80, 14.1 ± 5.5% of total colonies were positive for CRX, a photoreceptor precursor maker (Fig. 4H). To determine the potential for human iPSCs to express photoreceptor properties, we treated these cells with SFEB/DL, and subsequently with retinoic acid (1 μM) and taurine (100 μM), beginning at differentiation day 90. On day 120, we observed that 26.5 ± 8.3% of total colonies and 13.2 ± 1.6% of cells in those colonies were immunopositive for the photoreceptor marker recoverin. We also observed 49.9 ± 9.8% of recoverin positive cells co-expressed the rod photoreceptor marker rhodopsin (Fig. 4I–M). Taking together, we conclude that human iPSCs differentiate toward retinal fates with the differentiation method for human ES cells.

In this study, we have demonstrated that mouse and human iPSCs can be induced with defined factors to differentiate *in vitro* into retinal progenitors. Serum-free embryoid body-like cultures were used to induce neural differentiation of mouse and human iPSCs. Following treatment with Wnt and Nodal inhibitors, retinal progenitors positive for Rx, Pax6 and Mitf were evident. Subsequently, morphologically mature RPE-like cells were observed. Application of retinoic acid and taurine induced these cells to express the retinal photoreceptor markers Crx, recoverin, and rhodopsin. We conclude from this progression of the marker expression that these iPSCs differentiated into retinal progenitors and then putative photoreceptor and RPE cells. These differentiation conditions are the same that induced retinal progenitors, RPE and photoreceptors from ES cells [13].

In mouse ES cell cultures, we previously showed that $Rx^+/Pax6^+$ cells were observed on day 9 after differentiation was started. In this study with mouse iPS cell cultures, we could observe $Rx^+/Pax6^+$ cells not on day 9, but on day 15. The explanation for this result was not clear, but might have some relation to the condition of maintenance of mouse ES and iPS cells. The mouse ES cell line used in our previous study (EB5) was maintained in feeder-free, low concentration of FBS (5%) medium condition and appeared epithelia-like morphology. Although the cell line was selected by antibiotics resistant gene expression together with the expression of a pluripotent cell marker Oct3/4, the cell line may have a tendency of differentiation into ectoderm or neural lineage. The mouse iPS and ES cell lines (iPS-20D17 and RF8) that we used in this study were maintained with SNL feeder cells and in the medium containing 15% FBS, might take more time to neural and retinal differentiation.

We also previously showed that, in mouse ES cell cultures, DAPT, a Notch inhibitor, promotes photoreceptor differentiation in FACS-purified Rx^+ cells, although it has little effect on Rx^+ cells present in unpurified SFEB-treated cells. DAPT was not used in this study

because we considered that, similar to our previous study, DAPT would not effective on photoreceptor differentiation of mouse iPSCs without purification of Rx^+ cells.

In our differentiation condition, the differentiation efficiency of RPE and photoreceptors from human iPS cell cultures with cell lines 201B7 and 253G1 was not different from that human ES cell cultures. Therefore, in addition to their similarity in pluripotency, retinal differentiation methods using defined factors for ES cells are also applicable to iPSCs, although further research will be required to characterize the function of induced retinal cells.

The clinical applications for transplantation of cells cultured with materials from other animals, such as feeder cells or serum, are hampered by the risk of adverse immunologic response and potential exposure to xeno-pathogens. Thus, it is important to develop culture methods with defined factors that are free of animal-derived materials for the differentiation *in vitro* of cells required for transplantation. In the present study, we have succeeded in *in vitro* differentiation of both mouse and human iPSCs with the serum-free, feeder-free method, but the culture technique still includes animal-derived products such as KSR, N2 supplement, culture matrix and dissociation solutions. And it is also true that the production of iPS cell lines requires serum, KSR and feeder cells. Thus, we need to establish a xeno-free culture method for clinical application of iPSCs in cell transplantation therapy.

As for immune rejection, transplantation of patient-specific cells will have several advantages over comparable differentiated ES cells [10]. In exudative age-related macular degeneration, a retinal disease which causes severe visual deficits as a consequence of the patchy loss of RPE and disruption of the RPE-photoreceptor interface by the ingrowing subretinal fibrovascular tissue, introducing healthy RPE under the fovea and repair of Bruch's membrane may promote significant recovery of vision when performed in conjunction with surgical removal of subretinal fibrovascular tissue. However, allogenic RPE transplantation is likely to induce rejection of graft tissue in the absence of systemic immunosuppression [17]. Moreover, macular translocation surgery or autologous RPE and choroid patch translocation include a risk of serious surgical complications [7]. Therefore, transplantation of RPE cells derived from patient-specific iPSCs will have prominent advantages.

However, a risk of tumor formation by contaminating undifferentiated cells is not resolved [3]. Indeed, at least 0.6% of the mouse iPSCs remained undifferentiated in our cultures even 15 days after differentiation. Thus, to prevent tumor formation, establishment of purification methods will be requisite.

In summary, we demonstrated that iPSCs can differentiate into retinal-like cells with defined factors *in vitro* when induced with the same methodology used to differentiate ES cells. Future studies will be required to determine whether putative RPE and photoreceptors differentiated from iPSCs restore visual function when transplanted into the degenerative retina. Optimizing the differentiation of iPSCs and transplantation methods will facilitate the development of transplantation therapies for retinal diseases.

Acknowledgements

We thank Y. Sasai (RIKEN) for kindly providing Rx and Crx antibodies, A. Nomori, K. Iseki and C. Ishigami for technical assistance and the members of Takahashi laboratory for discussions. This work was supported by Grants-in-Aid from the Ministry of Education, Culture, Sports, Science and Technology of Japan (Y.H. and M.T.), the Mochida Memorial Foundation for Medical and Pharmaceutical Research (F.O.), and the Leading Project (M.T.)

Appendix A. Supplementary data

Supplementary data associated with this article can be found, in the online version, at doi:10.1016/j.neulet.2009.04.035.

References

[1] J. Aubert, H. Dunstan, I. Chambers, A. Smith, Functional gene screening in embryonic stem cells implicates Wnt antagonism in neural differentiation, Nat. Biotechnol. 20 (2002) 1240–1245.
[2] S. Chen, Q.L. Wang, Z. Nie, H. Sun, G. Lennon, N.G. Copeland, D.J. Gilbert, N.A. Jenkins, D.J. Zack, Crx, a novel Otx-like paired-homeodomain protein, binds to and transactivates photoreceptor cell-specific genes, Neuron 19 (1997) 1017–1030.
[3] H. Fukuda, J. Takahashi, K. Watanabe, H. Hayashi, A. Morizane, M. Koyanagi, Y. Sasai, N. Hashimoto, Fluorescence-activated cell sorting-based purification of embryonic stem cell-derived neural precursors averts tumor formation after transplantation, Stem Cells 24 (2006) 763–771.
[4] T. Furukawa, C.A. Kozak, C.L. Cepko, Rax, a novel paired-type homeobox gene, shows expression in the anterior neural fold and developing retina, Proc. Natl. Acad. Sci. U.S.A. 94 (1997) 3088–3093.
[5] T. Furukawa, E.M. Morrow, C.L. Cepko, Crx, a novel otx-like homeobox gene, shows photoreceptor-specific expression and regulates photoreceptor differentiation, Cell 91 (1997) 531–541.
[6] H. Ikeda, F. Osakada, K. Watanabe, K. Mizuseki, T. Haraguchi, H. Miyoshi, D. Kamiya, Y. Honda, N. Sasai, N. Yoshimura, M. Takahashi, Y. Sasai, Generation of $Rx^+/Pax6^+$ neural retinal precursors from embryonic stem cells, Proc. Natl. Acad. Sci. U.S.A. 102 (2005) 11331–11336.
[7] A.M. Joussen, F.M. Heussen, S. Joeres, H. Llacer, B. Prinz, K. Rohrschneider, K.J. Maaijwee, J. van Meurs, B. Kirchhof, Autologous translocation of the choroid and retinal pigment epithelium in age-related macular degeneration, Am. J. Ophthalmol. 142 (2006) 17–30.
[8] E.M. Levine, S. Fuhrmann, T.A. Reh, Soluble factors and the development of rod photoreceptors, Cell. Mol. Life. Sci. 57 (2000) 224–234.
[9] P.H. Mathers, A. Grinberg, K.A. Mahon, M. Jamrich, The Rx homeobox gene is essential for vertebrate eye development, Nature 387 (1997) 603–607.
[10] M. Nakagawa, M. Koyanagi, K. Tanabe, K. Takahashi, T. Ichisaka, T. Aoi, K. Okita, Y. Mochiduki, N. Takizawa, S. Yamanaka, Generation of induced pluripotent stem cells without Myc from mouse and human fibroblasts. Nat. Biotechnol. 26 (2007) 101–106.
[11] M. Nguyen, H. Arnheiter, Signaling and transcriptional regulation in early mammalian eye development: a link between FGF and MITF, Development 127 (2000) 3581–3591.
[12] K. Okita, T. Ichisaka, S. Yamanaka, Generation of germline-competent induced pluripotent stem cells, Nature 448 (2007) 313–317.
[13] F. Osakada, H. Ikeda, M. Mandai, T. Wataya, K. Watanabe, N. Yoshimura, A. Akaike, Y. Sasai, M. Takahashi, Toward the generation of rod and cone photoreceptors from mouse, monkey and human embryonic stem cells, Nat. Biotechnol. 26 (2008) 215–224.
[14] S. Parisi, D. D'Andrea, C.T. Lago, E.D. Adamson, M.G. Persico, G. Minchiotti, Nodal-dependent Cripto signaling promotes cardiomyogenesis and redirects the neural fate of embryonic stem cells, J. Cell Biol. 163 (2003) 303–314.
[15] K. Takahashi, S. Yamanaka, Induction of pluripotent stem cells from mouse embryonic and adult fibroblast cultures by defined factors, Cell 126 (2006) 663–676.
[16] K. Takahashi, K. Tanabe, M. Ohnuki, M. Narita, T. Ichisaka, K. Tomoda, S. Yamanaka, Induction of pluripotent stem cells from adult human fibroblasts by defined factors, Cell 131 (2007) 861–872.
[17] T.H. Tezel, L.V. Del Priore, A.S. Berger, H.J. Kaplan, Adult retinal pigment epithelial transplantation in exudative age-related macular degeneration, Am. J. Ophthalmol. 143 (2007) 584–595.
[18] K. Watanabe, D. Kamiya, A. Nishiyama, T. Katayama, S. Nozaki, H. Kawasaki, Y. Watanabe, K. Mizuseki, Y. Sasai, Directed differentiation of telencephalic precursors from embryonic stem cells, Nat. Neurosci. 8 (2005) 288–296.

Modeling Retinal Degeneration Using Patient-Specific Induced Pluripotent Stem Cells

Zi-Bing Jin[1,2☯], Satoshi Okamoto[1☯], Fumitaka Osakada[3], Kohei Homma[1], Juthaporn Assawachananont[1], Yasuhiko Hirami[1], Takeshi Iwata[4], Masayo Takahashi[1,5]*

1 Laboratory for Retinal Regeneration, RIKEN Center for Developmental Biology, Kobe, Japan, **2** School of Optometry and Ophthalmology, Eye Hospital, Wenzhou Medical College, Wenzhou, China, **3** Systems Neurobiology Laboratory, The Salk Institute for Biological Studies, La Jolla, California, United States of America, **4** National Institute of Sensory Organs, National Hospital Organization Tokyo Medical Center, Tokyo, Japan, **5** Center for iPS Research and Application, Kyoto University, Kyoto, Japan

Abstract

Retinitis pigmentosa (RP) is the most common inherited human eye disease resulting in night blindness and visual defects. It is well known that the disease is caused by rod photoreceptor degeneration; however, it remains incurable, due to the unavailability of disease-specific human photoreceptor cells for use in mechanistic studies and drug screening. We obtained fibroblast cells from five RP patients with distinct mutations in the *RP1*, *RP9*, *PRPH2* or *RHO* gene, and generated patient-specific induced pluripotent stem (iPS) cells by ectopic expression of four key reprogramming factors. We differentiated the iPS cells into rod photoreceptor cells, which had been lost in the patients, and found that they exhibited suitable immunocytochemical features and electrophysiological properties. Interestingly, the number of the patient-derived rod cells with distinct mutations decreased *in vitro*; cells derived from patients with a specific mutation expressed markers for oxidation or endoplasmic reticulum stress, and exhibited different responses to vitamin E than had been observed in clinical trials. Overall, patient-derived rod cells recapitulated the disease phenotype and expressed markers of cellular stresses. Our results demonstrate that the use of patient-derived iPS cells will help to elucidate the pathogenic mechanisms caused by genetic mutations in RP.

Citation: Jin Z-B, Okamoto S, Osakada F, Homma K, Assawachananont J, et al. (2011) Modeling Retinal Degeneration Using Patient-Specific Induced Pluripotent Stem Cells. PLoS ONE 6(2): e17084. doi:10.1371/journal.pone.0017084

Editor: Mark Mattson, National Institute on Aging Intramural Research Program, United States of America

Received October 28, 2010; **Accepted** January 15, 2011; **Published** February 10, 2011

Copyright: © 2011 Jin et al. This is an open-access article distributed under the terms of the Creative Commons Attribution License, which permits unrestricted use, distribution, and reproduction in any medium, provided the original author and source are credited.

Funding: This study was supported by the grant from the Ministry of Health, Labour and Welfare, Japan (#H21-Nanchi-Ippan-216). The funders had no role in study design, data collection and analysis, decision to publish, or preparation of the manuscript.

Competing Interests: The authors have declared that no competing interests exist.

* E-mail: mretina@cdb.riken.jp

☯ These authors contributed equally to this work.

Introduction

Retinitis pigmentosa (RP) leads inevitably to visual impairment due to irreversible retinal degeneration, specifically of primary rod photoreceptors. The condition causes night blindness and visual field defects. The disease onset spans a wide range of ages, but RP most often occurs in late life. There is no treatment that allows patients to avoid deterioration of visual function. RP encompasses a number of genetic subtypes, with more than 45 causative genes and a large number of mutations identified thus far. The genetic heterogeneity of RP suggests a diversity of disease mechanisms, which remain largely unclear. Furthermore, for many of the RP subtypes, no appropriate animal models are available. Although large clinical trials have been conducted with α-tocopherol and β-carotene, these studies found no statistically significant change of visual function in RP patients [1,2]. The underlying mutations causing disease in the patients tested in the clinical trials were not revealed, and the variability of individual responses to these drugs is unknown. One of the reasons why these clinical trials failed to examine the effectiveness of drugs is that the effect of a drug may be different between patients with different underlying mutations.

Induced pluripotent stem (iPS) cells reprogrammed from somatic cells [3,4] have enabled us to easily generate patient-derived terminally differentiated cells *in vitro* [5–7]. We have successfully induced differentiation of photoreceptor cells from both human embryonic stem (ES) cells [8] and iPS cells [9,10]. Modeling pathogenesis and treatment *in vitro* using patient iPS cell-derived photoreceptors will elucidate disease mechanisms; circumvent problems related to differences among species that arise when using animal models; decrease patient risk; and reduce the cost of early-stage clinical trials. Here, we generated iPS cells from RP patients with different mutations and demonstrated the potential of patient-derived photoreceptors for disease modeling.

Materials and Methods

RP patients and genetic mutations

The protocol of this study adhered to the tenets of the Declaration of Helsinki. The study was approved by the ethical committees of the Institute of Biomedical Research and Innovation Hospital and the RIKEN Center for Developmental Biology, Japan. Written informed consent from all patients was obtained. We selected five RP patients from four families whose disease-causing mutations have been identified (**Fig. 1A–D and Fig. S1**). Of the five RP patients in this study, three late-onset patients carried the following mutations: 721Lfs722X in *RP1*, W316G in *PRPH2*, and G188R in *RHO*. Two relatively early-onset patients from the same family carried a H137L mutation in *RP9*, which we

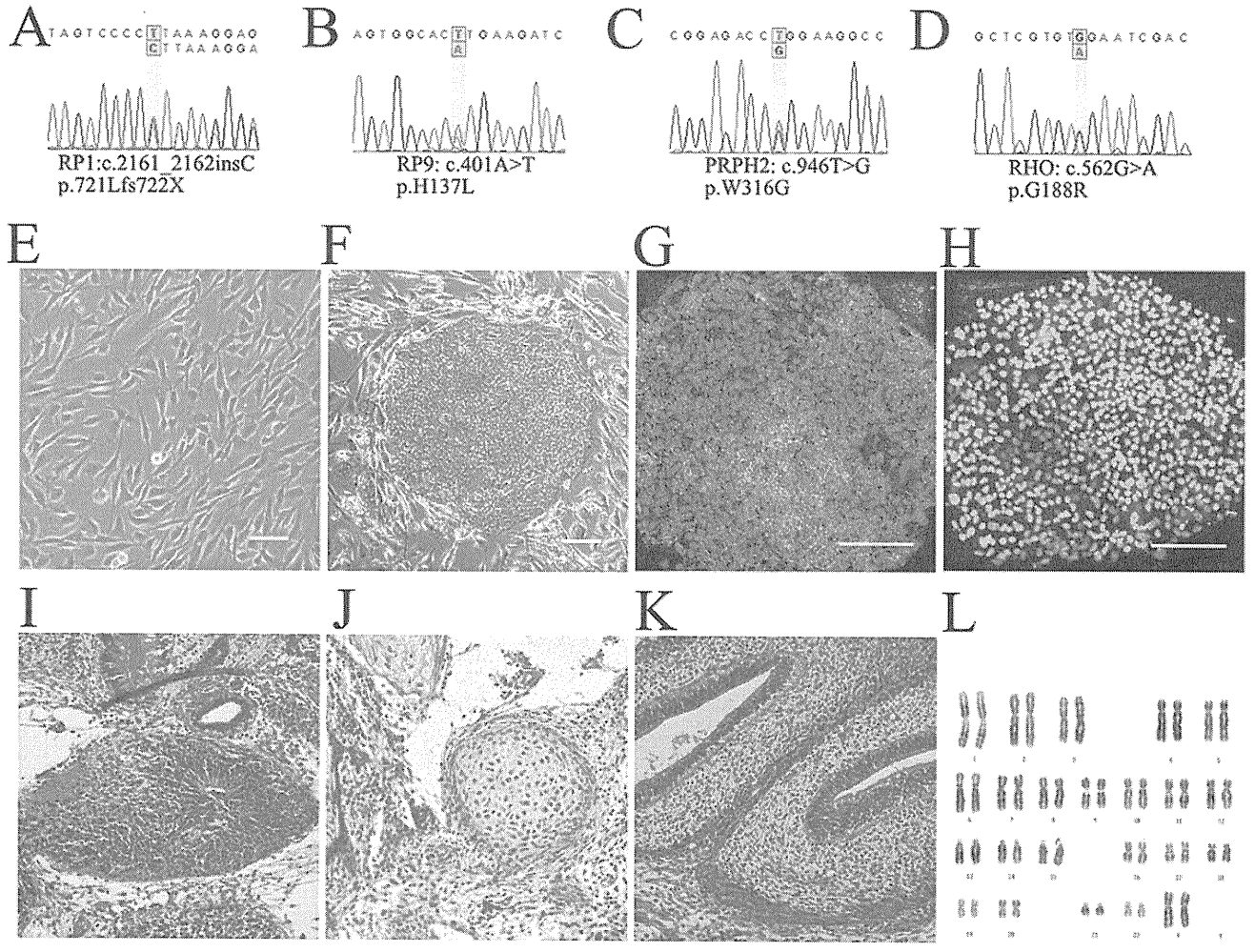

Figure 1. iPS cells derived from RP patients. Mutations identified in patients K21 (RP1) (**A**), K11 and K10 (RP9) (**B**), P101 (PRPH2) (**C**), and P59 (RHO) (**D**). Patient-derived fibroblast cells (**E**) were reprogrammed into iPS cells (**F**). The iPS cells expressed SSEA-4 (**G**) and Nanog (**H**). A teratoma formation test confirmed iPS cells' ability to generate all three germ layers: endoderm (**I**), mesoderm (**J**) and ectoderm (**K**). Karyotype analysis (**I**). Scale bars, 50 μm.
doi:10.1371/journal.pone.0017084.g001

confirmed by both genomic and cDNA sequencing (**Fig. S2**). All patients showed typical manifestations of RP (**Tab. S1**). Peripheral blood obtained from patients was used for DNA isolation. A comprehensive screening of disease-causing genes was carried out as described previously [11]. For the RP9 mutation, total RNA was isolated from fresh blood samples and iPS cells, and synthesized cDNA was subjected to PCR and direct sequencing to confirm whether the mutation was located in the *RP9* gene or the pseudo-RP9 gene (paralogous variant). Both fibroblast and iPS cells were analyzed to re-confirm the identified mutation.

iPS cells generation

To generate iPS cells, retroviral transduction of Oct3/4, Sox2, Klf4, and c-Myc into patient-derived fibroblast cells was carried out as described previously [3]. Established iPS cell lines were maintained on a feeder layer of mitomycin C-treated SNL cells (a murine-derived fibroblast STO cell line expressing the neomycin-resistance gene cassette and LIF) in a humidified atmosphere of 5% CO_2 and 95% air at 37°C. Cells were maintained in DMEM-F12 supplemented with 0.1 mM non-essential amino acids, 0.1 mM 2-mercaptoethanol, 2 mM L-glutamine, 20% KnockOut Serum Replacement (KSR), and 4 ng/ml basic fibroblast growth factor (Upstate Biotechnology).

Transgene quantification

To examine the copy number of transgenes integrated into the host genome, DNA was isolated and quantitative detection of viral transgenes was performed using real-time PCR. The endogenous gene was used as a control. Before quantitative PCR, a standard curve for each primer and/or probe set was determined using a set of plasmid DNA dilutions. Taqman qPCR to detect integrated OCT3/4, KLF4, and MYC was performed using 20 μl reactions consisting of 10 μl TaqMan Master Mix with uracil N-glycosylase, 4.9 μM primers, 250 nM probe, and 1 μl of the DNA sample. Quantification of viral SOX2 was assayed using SYBR Green.

Teratoma formation

Animal protocols were approved by the RIKEN Center for Developmental Biology ethical committee (No. AH18-05). A total of 10^7 trypsinized iPS cells were injected subcapsularly into the testis of SCID mice (two mice per iPS cell line). Four weeks later, the testis was fixed and sectioned for H&E staining.

Immunocytochemistry

Cells were fixed with 4% paraformaldehyde for 15 min at 4°C and then permeabilized with 0.3% Triton X-100 for 45 min. After 1 h blocking with 5% goat serum, cells were incubated with primary antibodies overnight at 4°C and subsequently with secondary antibodies for 1 h at room temperature. The primary and second antibodies used are listed in **Tab. S2**.

Karyotype analysis

Karyotype analysis of the iPS cell chromosomes was carried out using a standard G-band technique (300–400 band level).

Photoreceptor differentiation and drug testing

In vitro differentiation of rod photoreceptor cells was performed as previously reported [8], but with a minor modification. To find a KSR optimal for retinal differentiation, lot testing was conducted before differentiation. iPS colonies were dissociated into clumps with 0.25% trypsin and 0.1 mg/ml collagenase IV in PBS containing 1 mM $CaCl_2$ and 20% KSR. Feeder cells were removed by incubation of the iPS cell suspension on a gelatin-coated dish for 1 h. iPS clumps were moved to a non-adhesive MPC-treated dish (NUNC) in maintenance medium for 3 days, in 20% KSR-containing differentiation medium (DMEM-12 supplemented with 0.1 mM non-essential amino acids, 0.1 mM 2-mercaptoethanol, 2 mM L-glutamine) for 3 days, then in 15% KSR-containing differentiation medium for 9 days, and finally in 10% KSR-containing medium for 6 days. Cells were treated with Lefty-A and Dkk-1 during floating culture. At day 21, the cells were plated en bloc on poly-D-lysine/laminin/fibronectin−coated 8-well culture slides (BD Biocoat) at a density of 15–20 aggregates/cm^2. The cells were cultured in 10% KSR-containing differentiation medium until day 60. Cells were further treated with 100 nM retinoic acid (Sigma) and 100 μM taurine (Sigma) in photoreceptor differentiation medium (GMEM, 5% KSR, 0.1 mM non-essential amino acids, 0.1 mM 2-mercaptoethanol, 1 mM pyruvate, N2 supplement, and 50 units/ml penicillin, 20 μg/ml streptomycin). Differentiated cells from both normal and patient iPS cells were treated with 100 μM α-tocopherol, 200 μM ascorbic acid and 1.6 μM β-carotene starting at differentiation day 120. One week later, cells were fixed for immunostaining.

Electrophysiological recording

Recombinant lentiviral vectors expressing GFP under the control of the Nrl or RHO promoters were generated in HEK293t cells (RIKEN Cell Bank), and differentiated cells were infected with virus on day 90. Cells expressing GFP were targeted for patch clamp recordings. Voltage-clamp recordings were performed with 12–15 MΩ glass electrodes. Signals were amplified using Multiclamp 700B amplifiers (Molecular Devices). The internal solution was 135 mM K-gluconate, 10 mM HEPES, 3 mM KCl, 0.2 mM EGTA, 2.5 mM $MgCl_2$, 5 mM adenosine 5′-triphosphate, 0.3 mM guanosine-5′-triphosphate, 0.06 mM Alexa Fluor 594 (Molecular probes), adjusted to pH 7.6 with KOH. The retinal cells were perfused with oxygen-bubbled external medium: 23 mM $NaHCO_3$, 0.5 mM KH_2PO_4, 120 mM NaCl, 3.1 mM KCl, 6 mM Glucose, 1 mM $MgSO_4$, 2 mM $CaCl_2$, and 0.004% Phenol red. The medium was heated to 37°C with a temperature controller (Warner Instruments).

Cell count and statistical analysis

Differentiated cells visualized with specific antibodies were counted blindly by an independent observer. Data are expressed as means ± s.e.m. The statistical significance of differences was determined by one-way ANOVA followed by Tukey's test or Dunnett's test, or by two-way ANOVA followed by Bonferroni test using the GraphPad Prizm software. Probability values less than 0.05 were considered significant.

Results

Generation of iPS cell lines from patients with RP

Mutations identified in the five patients were confirmed by bi-directional sequencing (**Fig. S1**). Through genotyping of four patients and two normal relatives in the RP9 family, we found the H137L mutation in the *RP9* gene co-segregated with the disease, strongly indicating that the mutation is indeed the genetic cause of the disease. We cultured fibroblasts from skin samples of these patients on gelatin-coated dishes (**Fig. 1E**) and infected them with retroviral vectors encoding *OCT3/4* (also known as *POU5F1*), *SOX2*, *KLF4*, and *c-MYC*, using a previously established method [3]. Each mutation was re-confirmed in both fibroblasts and iPS cells. Established iPS colonies showed human embryonic stem cell-like morphology (**Fig. 1F and Fig. S3A**) and expressed pluripotency markers (**Fig. 1C–D**). We selected iPS cell lines for each patient using multiple criteria. First, we excluded iPS cell lines in which spontaneous differentiation occurred repeatedly during maintenance (**Fig. S3B**). We chose iPS colonies that maintained morphologies similar to those of human ES cells through more than 10 passages. Second, we quantified the transgene copy number and selected iPS cell lines with the fewest integrations, as the risk of gene disruption through random insertion increases with the number of transgenes (**Fig. S4A–E**). Third, in order to select iPS cell lines with full pluripotency, we verified the ability to form teratomas. Teratomas formed by injecting iPS colonies into the testis *in vivo* showed contributions to all three embryonic germ layers: ectoderm, mesoderm, and endoderm (**Fig. 1E–G**). Finally, karyotype analysis was carried out to examine the chromosome integrity. The patient-iPS cells showed normal karyotypes after extended passage, indicating chromosomal stability (**Fig. 1H**). These results provide *in vitro* and *in vivo* functional proof of pluripotency for RP patient-derived iPS cells.

Generation of patient-specific retinal photoreceptor

We previously demonstrated *in vitro* differentiation of retinal photoreceptor cells from wild-type human ES [8] and iPS cells [9,10] using a stepwise differentiation method known as serum-free culture of embryoid body-like aggregates [12]. We first evaluated the differentiation efficiency of three selected iPS cell lines of the five patients (**Fig. 2A**). Retinal progenitor, photoreceptor precursor, retinal pigment epithelium (RPE) and rod photoreceptor cells were sequentially induced (**Fig. 2B–K**), consistent with our previous studies [8–10,12]. All patient-derived iPS cell lines differentiated into RPE cells that form ZO-1+ tight junctions on differentiation day 60, with timing, morphology, and efficiency similar to that of wild-type iPS cells (**Fig. 2D–E; Fig. S5**). Immature photoreceptors expressing Crx and Recoverin (day ~60) were observed as clusters in the colonies (**Fig. S6A–B**). The patient-iPS cells also differentiated into blue Opsin+ or red/green Opsin+ cone photoreceptor cells (**Fig. 2H** and data not shown). Immunostaining of Rhodopsin (a marker of mature rod photoreceptors) revealed no Rhodopsin+ cells at differentiation day 100 (data not shown). Rhodopsin+ cells appeared at differentiation day 120 with a stable efficiency of the three independent iPS cell lines from each patient (**Fig. 2K,N and Fig. S6C**). Additionally, 15.1±0.60% and 13.3±1.65% cells were positive for Recoverin (a conventional marker for both rod, cone photoreceptors and cone bipolar cells) in K21- and K11-iPS cells, respectively

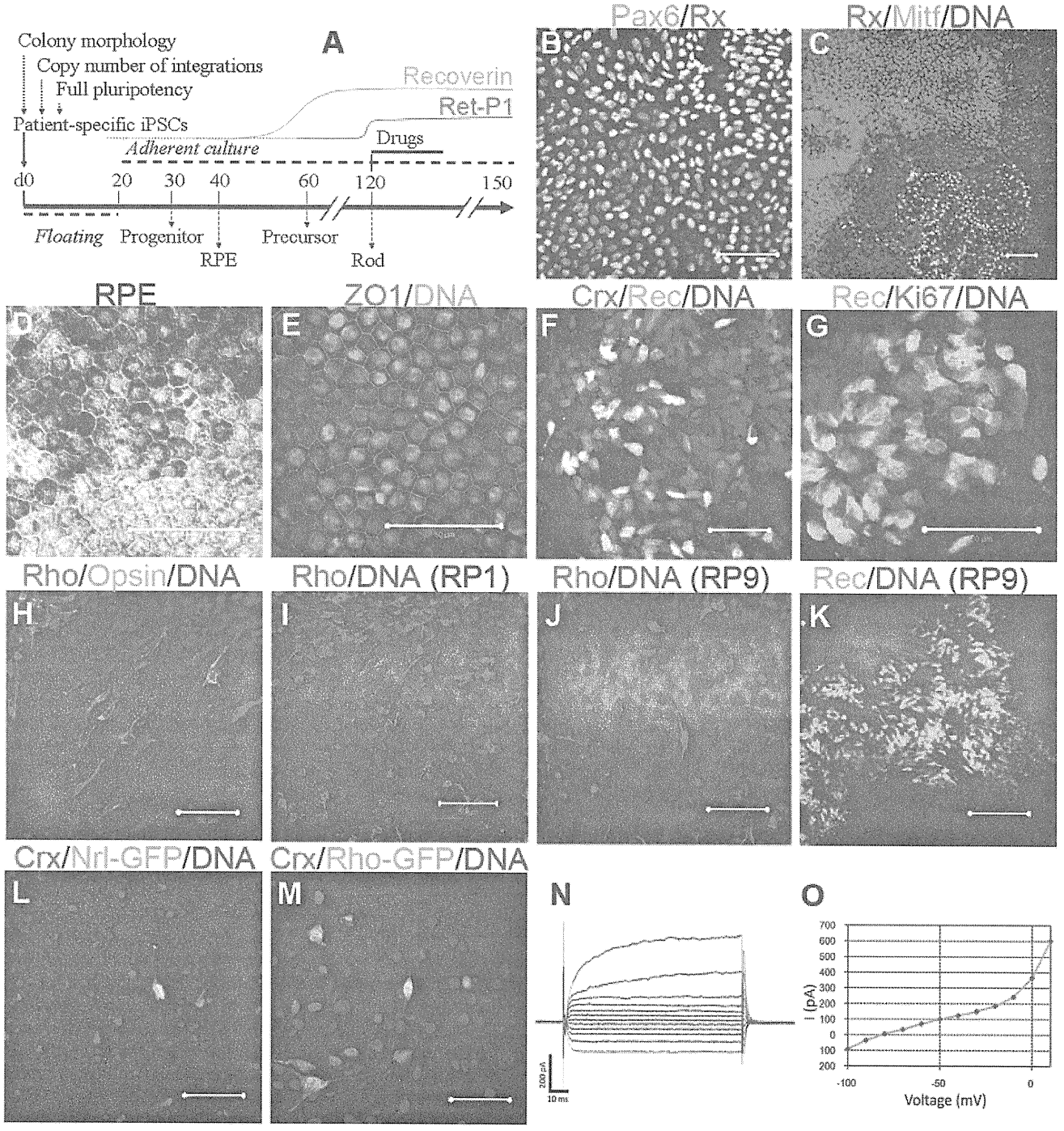

Figure 2. Induction of patient-specific retinal photoreceptor cells. Retinal cells were induced sequentially by *in vitro* differentiation. (**A**) Experimental schema. (**B**) Neural retina progenitor cells (Pax6+Rx+) and RPE progenitor cells (Mitf+) were separated in the culture dish (**C**). Patient-specific RPE cells exhibited hexagonal morphology and pigmentation (**D**) and expressed the tight junction marker ZO-1 (**E**). Photoreceptor cells were positive for immature photoreceptor markers Crx and Recoverin on day 60 (**F**). Recoverin+ cells did not co-express Ki67, a proliferating cell marker (**G**). Differentiation of rod photoreceptors (Rhodopsin+) and cone photoreceptors (Opsin+) from patient iPS cells (**H**). Rhodopsin + rod photoreceptors induced from K21-iPS at day 120 (**I**). K11-derived rod photoreceptors were observed at day 120 (**J**). No Rhodopsin+ cells were detected, but Recoverin+ cells were present at day 150(**K**). Induced rod photoreceptor cells (Crx+) labeled with lentiviral vectors encoding GFP driven by a rod photoreceptor-specific promoter Nrl (**L**: Nrl-GFP) or Rhodopsin (**M**: Rho-GFP). Arrows indicate cells co-expressing Crx and GFP. (**N**) Whole-cell recording of rod photoreceptor cell differentiated human iPS cells. Recorded cells expressed GFP under the control of the Rhodopsin promoter. (**O**) Relationship between voltage and membrane current (i) produced a non-linear curve, suggesting that voltage-dependent channels exist in iPS cell-derived rod photoreceptors Rec, Recoverin; Rho, Rhodopsin. Scale bars, 50 μm.
doi:10.1371/journal.pone.0017084.g002

(data from three selected lines), consistent with stable differentiation. Furthermore, we confirmed rod induction by labeling with lentiviral vectors driving GFP from the Rhodopsin and Nrl promoters, either of which is specifically expressed in rod photoreceptors (**Fig. 2L–M**). Whole-cell patch-clamp recording demonstrated that the rod photoreceptor cell membrane contains voltage-dependent channels, suggesting that differentiated patient-derived rod cells are electrophysiologically functional (**Fig. 2N–O**). Meanwhile, the excluded iPS cell lines (ones that showed spontaneous differentiation during maintenance, or had a high copy number of transgenes), demonstrated a significant diversity of differentiation (**Fig. S7**). Together, these data show that patient-derived iPS cells can differentiate into cells that exhibit many of the immunochemical and electrophysiological features of mature rod photoreceptor cells.

Patient-specific rod cells undergo degeneration *in vitro*

As compared with normal iPS cells, there is no significant difference in rod cell differentiation efficiency at day 120 in K21(RP1)-, P101(PRPH2)-, and P59(RHO)-iPS cell lines (**Fig. 3**). iPS cells from both K11(RP9) and K10(RP9) carried a RP9 mutation; however, rod cell number was significantly lower than in normal iPS cells (**Fig. 3**). We asked whether early death of precursor cells leads to a smaller number of mature rod photoreceptor cells. To determine whether genetic mutations induce degeneration in photoreceptors cells *in vitro*, we extended the culture period and evaluated the number of rod photoreceptors at day 150. In differentiated iPS cells from patient K21(RP1) at day 150, the number of Rhodposin+ cells was significantly decreased (**Fig. 3**). For the K11-iPS cells, no Rhodposin+ cells were found at day 150 (**Fig. 3**). Importantly, some K11-cells at day 150 were positive for Recoverin (10.3±1.99%) and Crx, markers for the rod, cone photoreceptors, and/or bipolar cells (**Fig. 2K** and data not shown), strongly suggesting that cone photoreceptor and/or bipolar cells survived, whereas the rod photoreceptors underwent degeneration *in vitro*. In addition, we detected cells positive for Islet1 (a marker for retinal amacrine, bipolar and ganglion cells), again consistent with the survival of other types of retinal cells (**Fig. S6F**). From these results, we concluded that mature rod photoreceptors differentiated from patient iPS cells selectively degenerate in an RP-specific manner *in vitro*.

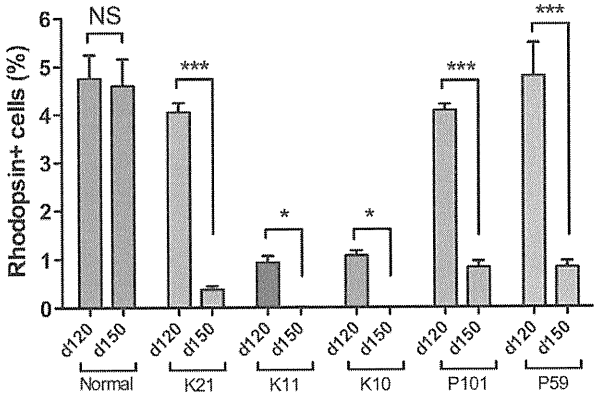

Figure 3. RP patient-derived rod photoreceptors undergo degeneration *in vitro*. iPS cells were differentiated into Rhodopsin+ rod photoreceptors in serum-free culture of embryoid body-like aggregates (SFEB culture). The percentages of Rhodopsin+ rod photoreceptors were evaluated at both day 120 and day 150, respectively. Data were from three independent iPS cell lines derived from the patients. ANOVA followed by Dunnett's test. * $p<0.05$; *** $p<0.001$. Values in the graphs are means and s.e.m.
doi:10.1371/journal.pone.0017084.g003

Cellular stresses involved in patient-derived rod cells

We next asked how the patient-derived rod photoreceptors degenerate. We evaluated apoptosis and cellular stresses in each cell line at both day 100 and day 120, respectively. Interestingly, in the RP9-iPS (K10 and K11) cells, a subset of Recoverin+ cells co-expressed cytoplasmic 8-hydroxy-2'-deoxyguanosine (8-OHdG), a major oxidative stress marker, indicating the presence of DNA oxidation in RP9 patient-derived photoreceptors by differentiation day 100 (**Fig. 4A** and **Fig. S8**). More caspase-3+ cells were presented in the Crx+ photoreceptor cluster of RP9-iPS than in those from other lines (**Fig. 4C–D**). After maturation of the rod photoreceptors from RP9-iPS cells, Rhodopsin+ cells co-expressed Acrolein, a marker of lipid oxidation (**Fig. 4E**), while no Rhodopsin+/Acrolein+ cells were observed in iPS cells derived from other patients carrying different mutations or in normal iPS cells (**Fig. 4F**). This pattern was similar to the cases of 8-OHdG and activated caspase-3. Thus, we conclude that oxidation is involved in the RP9-rod photoreceptor degeneration.

In differentiated RHO-iPS (P59) cells, we found that Rhodopsin proteins were localized in the cytoplasm (**Fig. 4G**), as determined by immunostaining with anti-Rhodopsin antibody (Ret-P1). This pattern is unlike the normal localization of Rhodopsin at the cell membrane in photoreceptors derived from normal iPS or other patient-derived iPS cells (**Fig. 4H** and data not shown). This result suggests accumulation of unfolded Rhodopsin, as reported previously in rhodopsin mutant mice cells [13]. We next examined the possible involvement of endoplasmic reticulum (ER) stress in RHO-iPS cell line degeneration. The Rhodopsin+ or Recoverin+ cells co-expressed immunoglobulin heavy-chain binding protein (BiP) or C/EBP homologous protein (CHOP), two conventional markers of endoplasmic reticulum (ER) stress, from day 120 (**Fig. 4I,K and Fig. S9**), while cells derived from control iPS or other mutant iPS cells were negative for BiP and CHOP (**Fig. 4J,L**). Taken together, these results demonstrate that ER stress is involved in rod photoreceptors carrying a RHO mutation.

Drug evaluation in patient-specific rod cells

The antioxidant vitamins α-tocopherol, ascorbic acid, and β-carotene have been tested in clinical trials as dietary therapies for RP [2] and in another major retinal degenerative disease, age-related macular degeneration [14]. Thus far, mostly due to the lack of appropriate validation models, there has been no evidence supporting the beneficial effects of these compounds on rod photoreceptors. We therefore assessed the effects of these agents on rod photoreceptors derived from patient iPS cells. In mouse retinal culture, short-term treatment with α-tocopherol, ascorbic acid and β-carotene at 100 μM, 200 μM and 1.6 μM, respectively, exerted no significant toxic effects on rod photoreceptor cells (**Fig. S10**). Since the differentiated rod photoreceptors underwent degeneration after day 120, we treated the cells for 7 days with these agents starting at day 120 (**Fig. 2A**). α-Tocopherol treatment significantly increased the number of Rhodopsin+ cells in iPS cells derived from K11- and K10-iPS with the RP9 mutation, while it had no significant effects on iPS cells with the either the RP1, PRPH2 or RHO mutation (**Fig. 5**). In contrast, neither ascorbic acid nor β-carotene treatment had any effect on iPS cells of any genotype (**Fig. S11**). We cannot currently explain the discrepancy between the effects of these antioxidants. It has been reported that under certain circumstances, anti-oxidants can act as "pro-oxidants" [15]. Taken together, our results indicate that treatment with α-tocopherol is beneficial to RP9-rod photoreceptor survival, and causes different effects on Rhodposin+ cells derived from different patients.

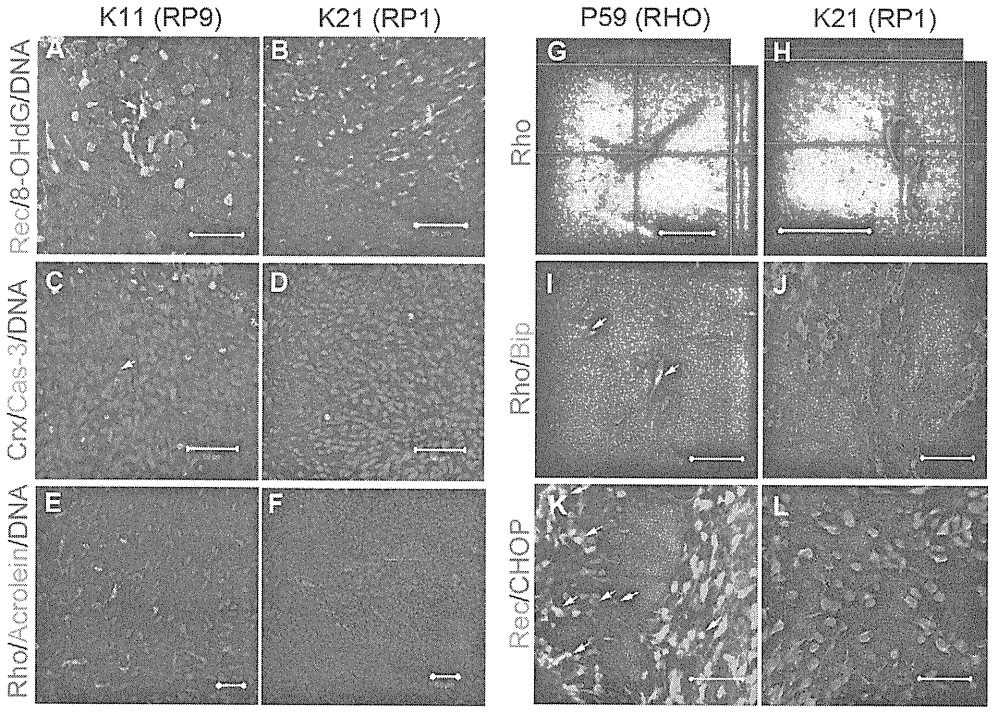

Figure 4. Cellular stress in patient-derived rod photoreceptor cells. Oxidative stress and apoptosis in differentiated rod photoreceptor cells derived from RP9-iPS (**A,C,E**) and RP1-iPS (**B,D,F**). (**A**) 8-OHdG, a marker for DNA oxidation, was found in K11- or K10-iPS–derived differentiated cells (day 100), but not in K21-iPS (**B**). Arrow indicates a cell double-positive for 8-OHdG and Recoverin. (**C**) The number of activated Caspase-3+ cells was greater in K11-iPS differentiation than in K21-iPS (**D**). From day 120, rod photoreceptor cells (Rhodopsin+) derived from RP9-iPS co-expressed the oxidative stress marker Acrolein (**E**); whereas RP1-iPS derivatives did not (**F**). (**G–L**) Abnormal cellular localization of Rhodopsin proteins and endoplasmic reticulum stress in RHO-iPS–derived rod photoreceptors. High magnification revealed cytoplasmic localization of Rhodopsin in rod photoreceptor cells carrying a RHO mutation (**G**) and a normal localization in the cell membrane in K21 cells (**H**). Rod cells derived from RHO-iPS co-expressed the ER stress markers BiP (**I**) and CHOP (**K**). K21-iPS–derived rod cells did not express BiP (**J**) or CHOP (**L**). Arrows indicate double-positive cells. Rec, Recoverin; Rho, Rhodopsin. All scale bars are 50 μm except for G and H (20 μm).
doi:10.1371/journal.pone.0017084.g004

Discussion

By using patient-derived iPS cells and *in vitro* differentiation technology, we have shown that RP9-retinitis pigmentosa is involved, at least in part, in oxidative stress pathways; this has not been reported previously in any animals or cell models. Furthermore, we have demonstrated that the antioxidant α-tocopherol exerts a beneficial effect on RP9-rod cells. Additionally, we have clearly shown that rod photoreceptors derived from patients with a RHO mutation are associated with ER stress; this is

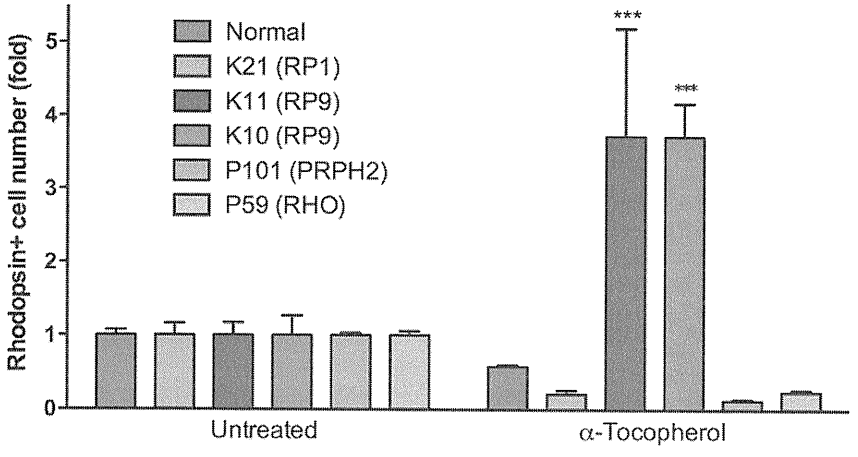

Figure 5. Disease modeling of patient-derived rod photoreceptor cells. α-Tocopherol treatment of patient-specific rod photoreceptors yielded a significant beneficial effect in RP9 mutant cells. Two-way ANOVA Bonferroni post-test showed no significance in other group (n = 3–8). Data represent 1–2 selected iPS cell lines of each patient. ***$p<0.001$. Values in the graphs are means and s.e.m.
doi:10.1371/journal.pone.0017084.g005

the first report of ER stress in a cell culture model for human rod cells. These cell models will be very useful for disease mechanism dissection and drug discovery. By screening several drugs that had already been tested in RP patients, we have revealed that rod photoreceptor cells derived from RP patients with different genetic subtypes exhibit significant differences in drug responses. Among the different types of antioxidants, α-tocopherol has either beneficial or non-beneficial effects on diseased photoreceptors, depending on the genetic mutation. This is the first report of the utilization of iPS cells related to personalized medicine, which will be helpful for routin clinical practice. Our results also provided evidence that genetic diagnosis is essential for optimizing personalized treatment for patients with retinal degenerative diseases [11]. An important future study made possible by this work is the screening of a compound library for drugs that could be used to treat RP. Patient-derived iPS cells revealed differences in pathogenesis and the efficacy of antioxidants among patients with different disease-causing mutations. Although the microenvironment affects the pathogenesis of diseases, and *in vitro* evaluation is not perfect, this study suggests that iPS cells could be used to select between multiple available treatments, allowing physicians to advise each patient individually. The weakness of our method for disease modeling is that differentiation requires a long period of time. Shortening the induction period and identifying appropriate surface markers for rod cells will improve disease modeling using patient-specific iPS cells.

In brief, we generated pluripotent stem cells from retinitis pigmentosa patients and induced them into retinal cells. Compared with normal cells, patient-derived rod cells simulated the disease phenotype and exhibited different responses to specific drugs. We found that patient-specific rod cells underwent degeneration *in vitro*, which maybe related to different cellular stresses. To our knowledge, this is the first report of disease modeling of retinal degeneration using patient-derived iPS cells.

Supporting Information

Figure S1 Pedigrees of K21 (A), P59 (B), K10 and K11 (C). Families of P59 (**B**) and K10 and K11 (**C**) show autosomal dominant mode of inheritance. (**C**) Mutation analysis was performed in four patients and two normal relatives in the RP9 family. The H137L mutation in RP9 gene was co-segregated with the disease in the family. Closed symbols indicate individuals with RP and open symbols indicate unaffected subjects. Question marks indicate symptom unknown. The bars above the symbols indicate examined subjects. Arrow, proband; slash, deceased.
(TIF)

Figure S2 Mutation in the *RP9* gene. (**A**) Alignment of RP9 sequence and pseudo-gene shows the same nucleotide in the mutated location. (**B**) Sequence chromatogram of cDNA sequence demonstrates the c.410A>T (H137L) mutation in the *RP9* gene, instead of the paralogous variant in pseudo-gene which was documented in RetNet (www.sph.uth.tmc.edu/retnet/disease.htm).
(JPG)

Figure S3 Selection by colony morphology. (**A**) iPS colony (K21S4) shows ES-like morphology. (**B**) Spontaneous differentiation in the colony during maintenance (K21S14). Scale bars, 50 μm.
(TIF)

Figure S4 Quantification of transgene copy number. Total copy number of four transgenes in the selected iPS lines. Selected iPS cells with fewest integrations and two high copy number lines used for *in vitro* differentiation.
(TIF)

Figure S5 Efficiency of RPE induction in patient-iPS cells. RPE production of the five patient-iPS cells showed no significant differences (n = 4). Data represent the percentage of RPE area at differentiation day 60. One-way ANOVA followed by Dunnett's test. Values are mean and s.e.m.
(TIF)

Figure S6 Induced retinal cells from patient iPS cells (K21S4). Crx+ photoreceptor precursor cells present in the cell cluster on differentiation day 60 (A). Crx+ cells co-expressed Recoverin, indicating differentiation into photoreceptor cells (B). Rhodopsin+ cells had a long process at day 150 (C). In the differentiated cells, we also observed cells positive of PKCα (a marker for bipolar cells) (D). Cells positive for Math5 and Brn3b (markers for ganglion progenitor or ganglion cells (day 60) (E). Cells positive for Islet-1 (a marker for amacrine, bipolar and ganglion cells) (F). Scale bars, 50 μm (A, D, E, and F); 20 μm (B and C).
(TIF)

Figure S7 Differentiation of the patient-iPS cells. iPS colony was cut into uniform sized pieces (**A**) and subjected to a floating culture (P59M8, day 20) (**B**). RPE (pigmented) and recoverin+ (green) cells were efficiently induced (P59M8, day 60) (**C**). (**D**) An excluded iPS line, P59M16, with high number transgenes showed a striking lentoid formation during the floating culture (day 20). Scale bars, 50 μm.
(TIF)

Figure S8 Oxidative stress in photoreceptor cells with the RP9 mutation (K11). (A) Recoverin, (B) 8-OHdG, (C) Recoverin/8-OHdG, (D) Recoverin/8-OHdG/DNA. Arrows indicate cells with weak Recoverin signal positive for 8-OHdG; Arrowheads represent cells with strong Recoverin signal positive for 8-OHdG; Asterisks represent Recoverin+ cells negative for 8-OHdG. Scale bar, 50 μm.
(JPG)

Figure S9 ER stress in photoreceptor cells with the RHO mutation (P59). (A) CHOP, (B) Recoverin, (C) Recoverin/CHOP, (D) Recoverin/CHOP/DNA. Arrows indicate cells with weak Recoverin signals positive for CHOP in nuclei; Arrowheads represent cells with strong Recoverin signals positive for CHOP; Asterisks represent Recoverin+ cells negative for CHOP. Scale bar, 50 μm.
(JPG)

Figure S10 Toxicity testing of the antioxidants in murine retina-derived rod photoreceptor cells. Primary culture of mouse retinal cells treated with 100 μM α-tocopherol, 200 μM ascorbic acid or 1.6 μM β-carotene for 24 hours and the rod photoreceptors were counted using flow cytometry. Value represents the ratio of treated-rod photoreceptors compared with control cells. n = 4. One-way ANOVA followed by Dunnett's test. Values are mean and s.e.m. NS, not significant.
(JPG)

Figure S11 Differentiated rod cells from normal and patient iPS cells treated with 200 μM ascorbic acid or 1.6 μM β-carotene did not show statistically significant differences. Two-way ANOVA Bonferroni post-test. Values are mean and s.e.m.
(JPG)

Table S1 Phenotypic data of the RP patients. M, male; F, female; AD, age at diagnosis; BCVA, best corrected visual acuity; HM, hand motion.
(DOC)

Table S2 Antibodies used in the present study.
(DOC)

Acknowledgments

We thank C. Ishigami and Y. Tada for assistance of mutation screening; K. Iseki, N. Sakai, Y. Wataoka, K. Sadamoto, A. Tachibana, C. Yamada for technical assistance; Y. Arata, W. Meng, C. Li, A. Suga, M. Mandai and all members in the Takahashi lab for advice.

Author Contributions

Conceived and designed the experiments: ZBJ MT. Performed the experiments: ZBJ SO FO KH JA. Analyzed the data: ZBJ SO FO. Contributed reagents/materials/analysis tools: MT YH TI. Wrote the paper: ZBJ MT.

References

1. Weleber RG, Gregory-Evans K (2006) Retinitis Pigmentosa and Allied Disorders. In: Hilton DR, Schachat AP, Ryan SJ, eds. Retina. Elsevier Mosby. pp 395–498.
2. Berson EL, Rosner B, Sandberg MA, Hayes KC, Nicholson BW, et al. (1993) A randomized trial of vitamin A and vitamin E supplementation for retinitis pigmentosa. Arch Ophthalmol 11: 761–772.
3. Takahashi K, Tanabe K, Ohnuki M, Narita M, Ichisaka T, et al. (2007) Induction of pluripotent stem cells from adult human fibroblasts by defined factors. Cell 131: 861–872.
4. Yu J, Vodyanik MA, Smuga-Otto K, Antosiewicz-Bourget J, Frane JL, et al. (2007) Induced pluripotent stem cell lines derived from human somatic cells. Science 318: 1917–1920.
5. Park IH, Arora N, Huo H, Maherali N, Ahfeldt T, et al. (2008) Disease-specific induced pluripotent stem cells. Cell 134: 877–886.
6. Raya A, Rodríguez-Pizà I, Guenechea G, Vassena R, Navarro S, et al. (2009) Disease-corrected haematopoietic progenitors from Fanconi anaemia induced pluripotent stem cells. Nature 460: 53–59.
7. Yamanaka S (2007) Strategies and new developments in the generation of patient-specific pluripotent stem cells. Cell Stem Cell 1: 39–49.
8. Osakada F, Ikeda H, Mandai M, Wataya T, Watanabe K, et al. (2008) Toward the generation of rod and cone photoreceptors from mouse, monkey and human embryonic stem cells. Nat Biotechnol 26: 215–224.
9. Osakada F, Jin ZB, Hirami Y, Ikeda H, Danjyo T, et al. (2009) In vitro differentiation of retinal cells from human pluripotent stem cells by small-molecule induction. J Cell Sci 122: 3169–3179.
10. Hirami Y, Osakada F, Takahashi K, Okita K, Yamanaka S, et al. (2009) Generation of retinal cells from mouse and human induced pluripotent stem cells. Neurosci Lett 458: 126–131.
11. Jin ZB, Mandai M, Yokota T, Higuchi K, Ohmori K, et al. (2008) Identifying pathogenic genetic background of simplex or multiplex retinitis pigmentosa patients: a large scale mutation screening study. J Med Genet 45: 465–472.
12. Ikeda H, Osakada F, Watanabe K, Mizuseki K, Haraguchi T, et al. (2005) Generation of Rx+/Pax6+ neural retinal precursors from embryonic stem cells. Proc Natl Acad Sci U S A 102: 11331–11336.
13. Sung CH, Davenport CM, Nathans J (1993) Rhodopsin mutations responsible for autosomal dominant retinitis pigmentosa. Clustering of functional classes along the polypeptide chain. J Biol Chem 268: 26645–26649.
14. van Leeuwen R, Boekhoorn S, Vingerling JR, Witteman JC, Klaver CC, et al. (2005) Dietary intake of antioxidants and risk of age-related macular degeneration. JAMA 294: 3101–3107.
15. van Helden YG, Keijer J, Heil SG, Picó C, Palou A, et al. (2009) Beta-carotene affects oxidative stress-related DNA damage in lung epithelial cells and in ferret lung. Carcinogenesis 30: 2070–2076.

Osteoarthritis and Cartilage (2009) **17,** 529–538
© 2008 Osteoarthritis Research Society International. Published by Elsevier Ltd. All rights reserved.
doi:10.1016/j.joca.2008.09.003

Osteoarthritis and Cartilage

International Cartilage Repair Society

OARSI OSTEOARTHRITIS

PGE2 signal *via* EP2 receptors evoked by a selective agonist enhances regeneration of injured articular cartilage

S. Otsuka M.D.†‡, T. Aoyama M.D., Ph.D.†*, M. Furu M.D.†§, K. Ito M.D.†‡, Y. Jin M.D.†, A. Nasu M.D.†§, K. Fukiage M.D.†§, Y. Kohno M.D., Ph.D.†§, T. Maruyama Ph.D.‖, T. Kanaji‖, A. Nishiura Ph.D.‖, H. Sugihara‖, S. Fujimura‖, T. Otsuka M.D., Ph.D.‡, T. Nakamura M.D., Ph.D.§ and J. Toguchida M.D., Ph.D.†

† *Department of Tissue Regeneration, Institute for Frontier Medical Sciences, Kyoto University, Kyoto, Japan*
‡ *Department of Orthopaedic Surgery, Graduate School of Medical Sciences, Nagoya City University, Nagoya, Japan*
§ *Department of Orthopaedic Surgery, Graduate School of Medicine, Kyoto University, Kyoto, Japan*
‖ *Ono Pharmaceutical Co. Ltd., Osaka, Japan*

Summary

Objective: The effect of the prostaglandin E2 (PGE2) signal through prostaglandin E receptor 2 (EP2) receptors on the repair of injured articular cartilage was investigated using a selective agonist for EP2.

Methods: Chondral and osteochondral defects were prepared on the rabbit femoral concave in both knee joints, and gelatin containing poly-lactic-co-glycolic acid microspheres conjugated with or without the EP2 agonist was placed nearby. Animals were sacrificed at 4 or 12 weeks post-operation, and regenerated cartilage tissues and subchondral structure remodeling were evaluated by histological scoring. The quality of regenerated tissues was also evaluated by the immunohistochemical staining of EP2, type II collagen, and proliferating cell nuclear antigen (PCNA). As an evaluation of side effects, the inflammatory reaction of the synovial membrane was analyzed based on histology and the mRNA expression of matrix metalloproteinase3 (MMP3), tissue inhibitor of metalloproteinase 3 (TIMP3), and interleukin-1β (IL-1β). Also, the activity of MMP3 and the amount of tumor necrosis factor-α (TNF-α) and C-reactive protein in joint fluid were measured.

Results: In both models, the EP2 agonist enhanced the regeneration of the type II collagen-positive tissues containing EP2- and PCNA-positive chondrocytes, and the histological scale of regenerated tissue and subchondral bone was better than that of on the control side, particularly at 12 weeks post-operation. No inflammatory reaction in the synovial membrane was observed, and no induction of pro-inflammatory cytokines was found in joint fluid.

Conclusion: Selective stimulation of the PGE2 signal through EP2 receptors by a specific agonist promoted regeneration of cartilage tissues with a physiological osteochondral boundary, suggesting the potential usefulness of this small molecule for the treatment of injured articular cartilages.
© 2008 Osteoarthritis Research Society International. Published by Elsevier Ltd. All rights reserved.

Key words: PGE2, EP2, Agonist, Cartilage, Defect, Repair, Therapeutic drug, Osteoarthritis.

Introduction

Chondrocytes in articular cartilage are differentiated cells with minimum proliferating potential and low metabolic activity[1]. Because these cells are fully responsible for the production of cartilage matrix consisting of collagens and proteoglycans, considerable damage to articular cartilage is unrepairable, initiating a sequence of catabolic events leading to a pathological condition known as osteoarthritis (OA). Although inflammation of the synovium and the destruction of subchondral bone integrity also play an important role in the progression of OA, the poor regenerative capacity of chondrocytes is the major disease-causing factor[1,2]. In the early stages of OA, however, not only catabolic but also anabolic activity is enhanced in chondrocytes. As catabolic activity, chondrocytes produce several catabolic cytokines such as interleukin-1 (IL-1), which in turn induce the production of proteinases such as matrix metalloproteinases (MMPs) and a disintegrin-like and metalloprotease with thrombospondin (ADAMTS) leading to the destruction of the matrix network[2]. As anabolic activity, chondrocytes produce anabolic cytokines such as the bone morphogenic protein (BMP) family and insulin like growth factor-1 (IGF-1), which induce the synthesis of collagens and initiate the proliferation of chondrocytes themselves making osteophytes at the periphery[2]. A disruption of the equilibrium between the catabolic and anabolic activities results in catastrophic damage to articular cartilage. In adult articular cartilage, the equilibrium leans toward catabolic activity; the proliferation of chondrocytes is decreased and the subchondral structure is weak.

The role of prostaglandin E2 (PGE2) in the development of OA is controversial. Pro-inflammatory signal mediators such as IL-1 and tumor necrosis factor-α (TNF-α) induce

*Address correspondence and reprint requests to: Dr T. Aoyama, M.D., Ph.D., Department of Tissue Regeneration, Institute for Frontier Medical Sciences, Kyoto University, 53 Kawahara-cho, Shogoin, Sakyo-ku, Kyoto 606-8507, Japan. Tel: 81-75-751-4107; Fax: 81-75-751-4646; E-mail: blue@frontier.kyoto-u.ac.jp
Received 13 April 2008; revision accepted 2 September 2008.

the synthesis of PGE2 by promoting the expression or activities of cycloxygenase (COX)-2 and microsomal PGE synthase-1[3]. The synthesized PGE2 promotes IL-1 expression as a positive feedback mechanism, degrades the cartilage matrix[4], and finally induces apoptosis of chondrocytes[5], indicating a catabolic role for PGE2 in OA. In some reports, however, anabolic effects of PGE2 were demonstrated[1,3]. PGE2 opposed the effect of IL-1 by down-regulating type I collagen[6] and stimulating type II collagen gene expression[7,8]. Also, PGE2 stimulated the synthesis of proteoglycan and collagen through the induction of IGF-1-binding protein[9], and induced the proliferation of rat chondrocytes as demonstrated by an increase in the incorporation of [^{3}H]-thymidine[9].

Several factors are involved in these controversial findings including experimental design, the level of PGE2 expression, the balance with other pro-inflammatory cytokines, and most notably, the variety of receptors. PGE2 exerts its biological effect through one of four receptors, EP1, EP2, EP3, or EP4. The development of specific agonists and antagonist for each receptor enables the understanding of the receptor-specific signal transduction mechanism and its consequence. Signals through EP1 and EP3 coupled by G_i protein increase the intra-cellular Ca^{2+} concentration, and those through EP2 and EP4 coupled by G_s protein increase cyclic adenosine monophosphate (cAMP). Although the second messenger is common, the amide acid identity is only 31% between EP2 and EP4. EP4 (513 amino acids) has the longest intra-cellular C terminal, but EP2 (362 amino acids) has a compact structure. In osteoclastogenesis, the EP2 and EP4 mediate the induction of receptor activator of nuclear factor-kappa B (NF-κB) ligand (RANKL), but the extent of the contribution by each receptor is different. Although both EP2 and EP4 are expressed in dendritic cell, EP4 has selective action for cell migration. This selectivity of EP4 may be caused by the fact that EP4 but not EP2 couples to phosophatidylinositol 3-kinase in addition to cAMP[10].

We have previously demonstrated that EP2 was the major PGE2 receptor in articular chondrocytes[11]. And a specific agonist for EP2 not EP4 promoted the growth of mouse and human chondrocytes by up-regulating the expression of growth-promoting genes such as the *cyclin D* gene stimulating the increase of cAMP[11]. The protein structure and function of EP2 are conserved between many species, and the amino acid homology between the human and mouse, rat, or rabbit is 88.2, 84.9, and 90.2%, respectively. The effect of the EP2 agonist on chondrocytes was confirmed in a rat organ culture system, suggesting the possible application of this small molecule as a new therapeutic tool for injured articular cartilage[11].

In this study, we investigated the effect of an EP2 agonist on injured articular cartilage *in vivo* using rabbit knee joints and also on other joint structures such as the synovium and subchondral bone.

Materials and methods

REAGENTS

Microspheres loaded with the selective EP2 agonist, ONO-8815Ly[12] prepared by the emulsion–solvent evaporation method as described[13]. Briefly, ONO-8815Ly was dissolved in purified water as the inner water phase and polylactic-co-glycolic acid (PLGA) was dissolved in dichloromethane as the oil phase. The water/oil (w/o) emulsion was gradually added to the outer water phase containing polyvinyl alcohol (PVA, 0.1%, w/v), NaCl (2%, w/v) and maltose (2%, w/v) adjusted to pH 3.0, under stirring with a turbine-shaped mixer at 5000 rpm to obtain a water/oil/water emulsion. Then PLGA microspheres were formed in the outer water phase after the evaporation of dichloromethane. In order to recover the microspheres without a free form of ONO-8815Ly, the suspension was centrifuged at 3000 rpm for 10 min and the microspheres were precipitated. The washed microsphere precipital was lyophilized to remove residual organic solvent and water, and then dried solid ONO-8815Ly-loaded microspheres were recovered. ONO-8815Ly-loaded microspheres were dispersed in purified water, and then gelatin aqueous solution (20%, w/w) was poured into the microsphere suspension. The resultant microsphere–gelatin suspension was poured into a polypropylene container and placed in a refrigerator for 12 h to form a gel. Afterward, glutaraldehyde aqueous solution (12.5 μg/ml) was poured into the microsphere–gelatin gel and placed in the refrigerator for 24 h for the crosslink reaction. The gel sheet obtained was placed into glycine aqueous solution. These procedures were performed repeatedly. Small cylinder-shaped gelatin hydrogels containing either 80 or 400 μg of ONO-8815 were obtained by hollowing out the gelatin hydrogel sheet.

SURGICAL PROCEDURE

The institutional animal research committee, according to the guidelines for Animal Experiments of Kyoto University, approved this investigation. Japanese white rabbits (Shimizu Laboratory Supplies Co., Kyoto, Japan) were at least 5 months old and had a body weight of 3 kg.

Two types of cartilage defect on the femoral concave of the patello-femoral joint were made according to depth (Supplementary Fig. 1). A chondral defect, which involved the osteochondral boundary (tide mark) but not subchondral bone, was made using a punch without damaging the subchondral bone (5.0 mm in diameter) [Supplementary Fig. 1(A–C)]. An osteochondral defect was made using a hand drill [4.0 mm in diameter and 5.0 mm in depth, Supplementary Fig. 1(D–F)]. By preliminary experiments, we have confirmed that both types of defects were not healed spontaneously (data not shown).

The same type of defect was created in both femurs, and a cylinder-shaped gelatin hydrogel containing PLGA microspheres conjugated with ONO-8815 (80 or 400 μg) was placed into the infra-patellar fat pad on one side (thereafter designated EP2 agonist-treated samples), and gelatin hydrogels without microspheres were placed on the contralateral side (contralateral samples). The animals were allowed to move. To exclude any possible effect of ONO-8815 in the systemic circulation, controls were established, in which empty gelatin hydrogel was placed in bilateral knee joints after creating each defect model (control samples, $N=3$). Animals were sacrificed and evaluated at 4 ($N=5$) and 12 ($N=8$) weeks after the operation.

HISTOLOGICAL EVALUATION

Cartilage samples were fixed overnight at 4°C in a 10% formalin solution, decalcified by formic acid, and embedded in paraffin. Then sections were cut at 6 mm through the center of each defect, stained with Safranin-O/Fast Green and hematoxylin–eosin (HE), examined in a blinded manner by two evaluators, and graded with the use of a modified Wakitani histological scale[14]. The reconstitution of articular chondrocytes and subchondral bone connections (category II on the modified Wakitani scale) was partially evaluated by grading from 0 to 7. Specimens of the synovium around the infra-patellar fat pads were fixed in 10% formalin, embedded in paraffin, and cut into 6 μm thick sections for histological evaluation. Sections were stained with HE and the severity of synovial lesions was graded according to the histological scoring system, based on the hyperplasia of synovial lining cells, hypertrophy of the synovial lining layer, infiltration of inflammatory cells, proliferation of granulation tissue, and vascularization[15]. Two independent observers blinded to the treatment groups graded all sections.

IMMUNOHISTOCHEMISTRY

Immunostaining of proliferating cell nuclear antigen (PCNA; diluted 1:100; Dako, Glostrup, Denmark) and alpha1 type II collagen (diluted 1:50; Daiichi Fine Chemical, Toyama, Japan) was performed as previously mentioned[11]. Immunostaining of EP2 (diluted 1:100; Cayman Chemical Co., Ann Arbor, MI) was performed as described by Fukuda *et al.*[16]. Under the microscope (400×), all cells and PCNA-positive cells were counted by two individuals. Three visual fields were randomly selected by each observer, and, therefore, each specimen was evaluated three times. Then labeling index was calculated as the mean of these three values. The relative increase in PCNA-positive cells was expressed as the ratio of the labeling index of the EP2 agonist-treated sample vs that of the contralateral sample. The labeling index of control sample was also calculated as a value relative to those of contralateral sample.

ASSAY OF MMP3, TNF-α, AND C-REACTIVE PROTEIN (CRP) IN SYNOVIAL FLUID

After the injection of 1 ml of saline solution into the knee joint, synovial fluid was obtained by arthrocentesis through a sub-patellar approach. Synovial fluid was aspirated as far as possible from the knee joint. After

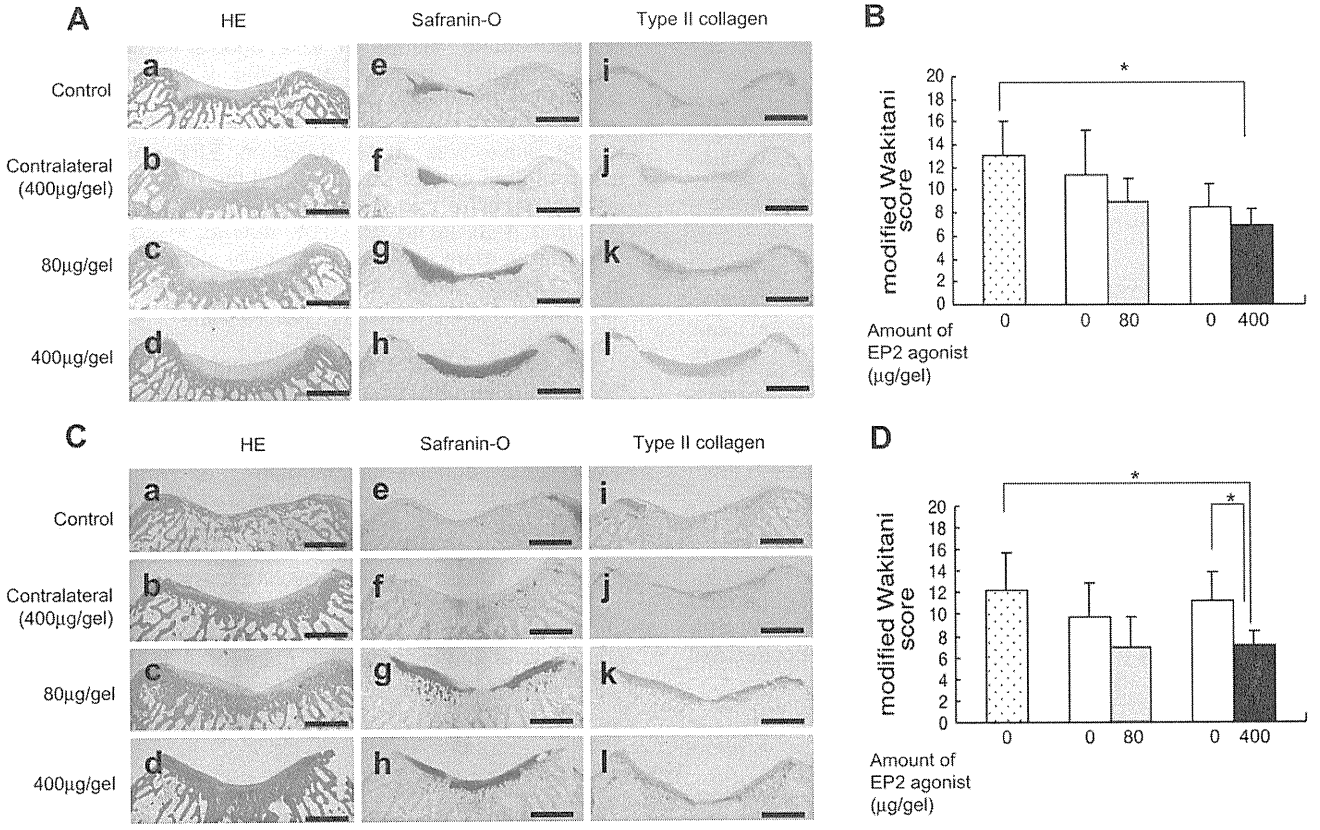

Fig. 1. Effects of EP2 agonist on the regeneration of chondral defects. Histological evaluations were performed at 4 (A) or 12 (C) weeks after the operation. Each specimen was prepared from control samples (a, e, and i), contralateral (b, f, and j), or EP2 agonist-treated (c, g, and k, 80 μg/gel; d, h and l; 400 μg/gel) samples. The quality of regenerated tissues was analyzed by HE staining (a–d), Safranin-O staining (e–h), or immunohistochemical staining with anti-type II collagen Ab (i–l). Magnification 2×. Bar = 2.0 mm. The quality of regenerated tissues was also evaluated with a modified Wakitani histological scale at 4 (B) and 12 (D) weeks after the operation. Dotted and open boxes indicate the scale for control and contralateral samples, respectively, $^*P < 0.05$.

the specimen was centrifuged at 1500 rpm for 20 min, the supernatant was drawn out and stored at −70°C[17]. MMP3 activity was measured with a MMP3 fluorimetric drug discovery kit (BIOMOL International LP, Plymouth Meeting, PA). TNF-α levels in joint fluids were measured using a sandwich enzyme-linked immunosorbent assay (ELISA) with specific anti-TNF-α polyclonal antibodies (Abs) (BD Pharmingen, San Diego, CA). Briefly, microtiter plates were coated with 50 μl of anti-rabbit. TNF-α capture Abs (4 mg/ml) overnight at 4°C, then washed twice with phosphate buffered saline (PBS) containing 0.05% Tween 20 and blocked overnight at 4°C with 10% fetal bovine serum (FBS) in PBS. After the plates were washed four times, standards and samples (100 μl) were incubated in duplicate overnight at 4°C. Plates were again washed and a biotin-conjugated anti-TNF-α secondary Ab (2 mg/ml) was added for 1 h at room temperature. A 30-min incubation with a 1:400 dilution of avidin–peroxidase (Sigma) followed extensive washing of the plate. Finally, TMBlue (Intergen, Milford, MA) substrate was added (100 μl/well) and incubated at room temperature for 30 min. The absorbance was read at 450 nm with an UVmax microplate reader (Molecular Devices, Menlo Park, CA). Rabbit CRP was measured with a rabbit CRP ELISA kit (Alpha Diagnostic International Inc., San Antonio, TX).

REVERSE TRANSCRIPTION-POLYMERASE CHAIN REACTION (RT-PCR)

Total RNA was extracted from frozen synovial samples using TRIzol reagent (Invitrogen, Carlsbad, CA) and 1 μg was reverse transcribed for single-stranded cDNA using the oligo (dT) primer and Superscript II reverse transcriptase (Invitrogen). RT-PCR was performed in duplicate for each sample using primers listed in Table I[18,19].

Table I
Primers used in the RT-PCR analyses

Gene	Primers*	Size (bp)	Position	Accession no.
MMP3	CTGGAGGTTTGATGAGAAGA CAGTTCATGCTCGAGATTCC	336	1278–1297 1597–1616	NM_001082280
TIMP1	GCAACTCCGACCTTGTCATC AGCGTAGGTCTTGGTGAAGC	326	122–141 428–447	NM_001082232
IL-1β	TGCTGTCCAGACGAGGGCAT ACTCTCCAGCTGCAGGGTAG	473	210–229 664–683	NM_001082201
GAPDH	GTCAAGGCTGAGAACGGGAA GCTTCACCACCTTCTTGATG	613	246–265 839–858	NM_001082253

*All primer sequences are written from 5′ to 3′. The top sequence is the sense primer and the bottom sequence is the anti-sense primer.

QUANTITATIVE RT-PCR

The levels of mRNA expression of genes (*MMP3*, *TIMP1*, *IL-1β* and *glyceraldehyde 3-phosphate dehydrogenase* (*GAPDH*)) were quantified by SYBR Green (Applied Biosystems, Foster City, CA) real time PCR with the ABI PRISM 377 Sequence Detection System (Applied Biosystems). Each gene amplification efficiency was similar with *GAPDH*. All reactions were run in triplicate, and the mean value was used to calculate the ratio of target gene/*GAPDH* expression in each sample. Using the ratio in untreated sample as a standard (1.0), the relative ratio of the treated sample was presented as the relative expression level of the target gene[11].

STATISTICAL ANALYSES

All statistical analyses were performed using Statcel software. The results are shown as the mean ± SD. The analysis of variance (ANOVA) test was used to compare the differences in the scales between multiple groups. The Student's *T* test was used to compare the differences in the scales between two groups. A P value < 0.05 was considered significant.

Results

EP2 AGONIST PROMOTED TISSUE REGENERATION IN THE CHONDRAL DEFECT MODEL

Four weeks after the operation, the quality of regenerated tissues was analyzed by HE staining [Fig. 1(A, a–d)], Safranin-O staining [Fig. 1(A, e–h)], or immunohistochemical staining with anti-type II collagen Ab [Fig. 1(A, i–l)]. Most of regenerated tissues in EP2 agonist-treated samples were Safranin-O-positive and type II collagen-positive, suggesting the quality as hyaline cartilage. The quality of regenerated tissue evaluated by modified Wakitani histological scale was much better in EP2 agonist-treated samples than control samples, and the difference was statistically significant in the case of 400 μg/gel-treated samples [Fig. 1(B): 80 μg, $P = 0.08$; 400 μg, $P = 0.04$]. On the other hand, there were no statistically significant difference in histological scale between EP2 agonist-treated and contralateral samples [Fig. 1(B): 80 μg, $P = 0.21$; 400 μg, $P = 0.24$].

The effect of EP2 agonist treatment was much clear at 12 weeks after operation. In control and contralateral samples, the amount of regenerated tissues was much less than that found at 4 weeks after operation, and most of them were negative for Safranin-O or type II collagen [Fig. 1(C)]. In EP2 agonist-treated samples, regenerated tissues reached a considerable width, most of which were Safranin-O and type II collagen-positive indicating properties compatible with hyaline cartilage [Fig. 1(C)]. The histological scale of EP2 agonist-treated samples showed significantly better than that of control and also contralateral samples in the case of 400 μg/gel-treated

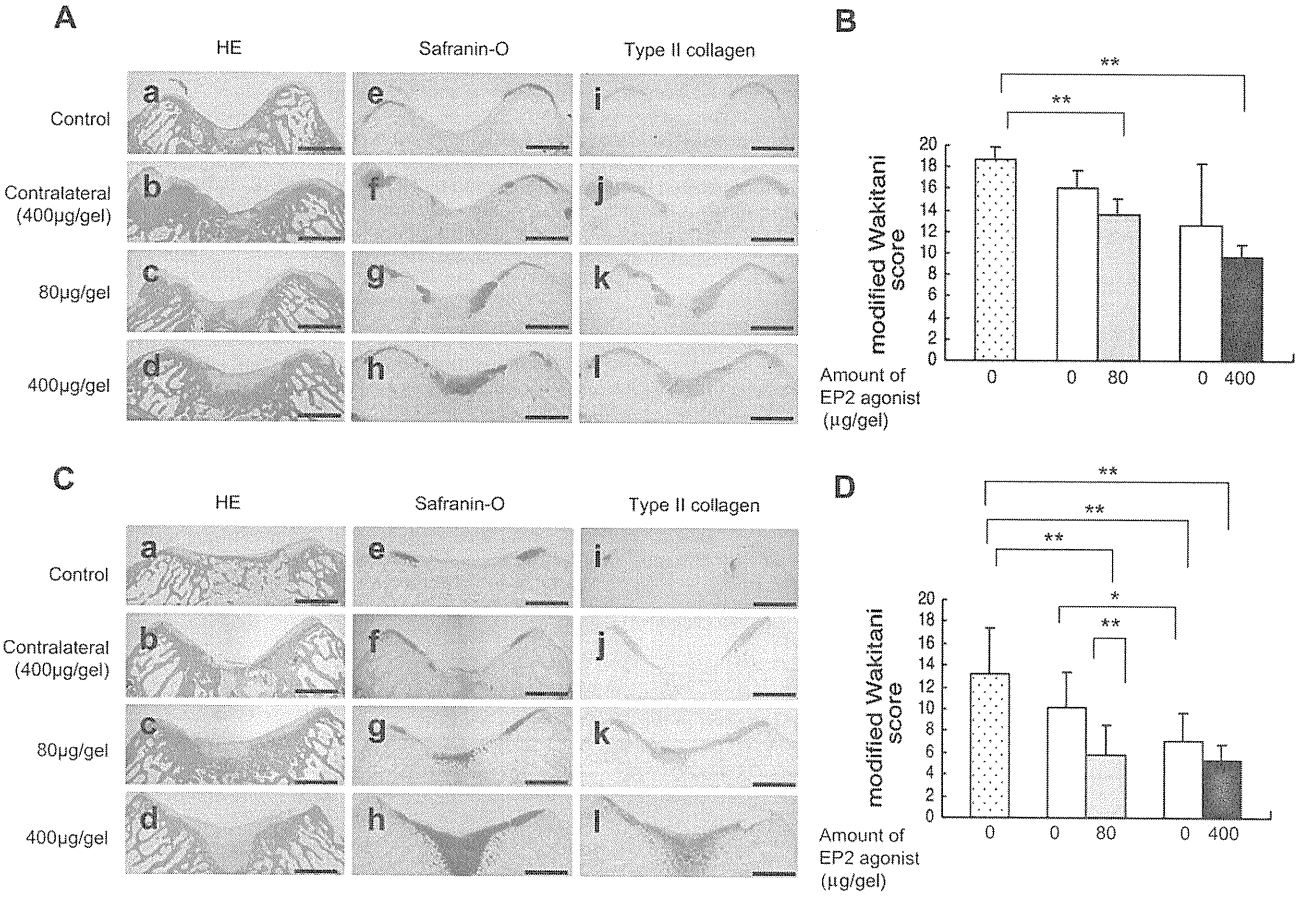

Fig. 2. Effects of EP2 agonist on the regeneration of osteochondral defects. Histological evaluations were performed at 4 (A) or 12 (C) weeks after the operation. Each specimen was prepared from control samples (a, e, and i), contralateral (b, f, and j), or EP2 agonist-treated (c, g, and k, 80 μg/gel; d, h and l; 400 μg/gel) samples. The quality of regenerated tissues was analyzed by HE staining (a–d), Safranin-O staining (e–h), or immunohistochemical staining with anti-type II collagen Ab (i–l). Magnification 2×. Bar = 2.0 mm. The quality of regenerated tissues was also evaluated with a modified Wakitani histological scale at 4 (B) and 12 (D) weeks after the operation. Dotted and open boxes indicate the scale for control and contralateral samples, respectively, $^{**}P < 0.01$; $^{*}P < 0.05$.

samples [Fig. 1(D): vs control, $P = 0.02$; vs contralateral, $P = 0.01$]. The histological scale of contralateral samples tended to be better than that of control samples, although there was no statistical significance [Fig. 1(C): 80 μg, $P = 0.31$; 400 μg; $P = 0.1$, Fig. 1(D): 80 μg, $P = 0.2$; 400 μg; $P = 0.35$].

EP2 AGONIST PROMOTED TISSUE REGENERATION IN THE OSTEOCHONDRAL DEFECT MODEL

To analyze the effect of the EP2 agonist on tissue regeneration in osteochondral lesions, an osteochondral defect model was created [Supplementary Fig. 1(C–E)]. At 4 weeks

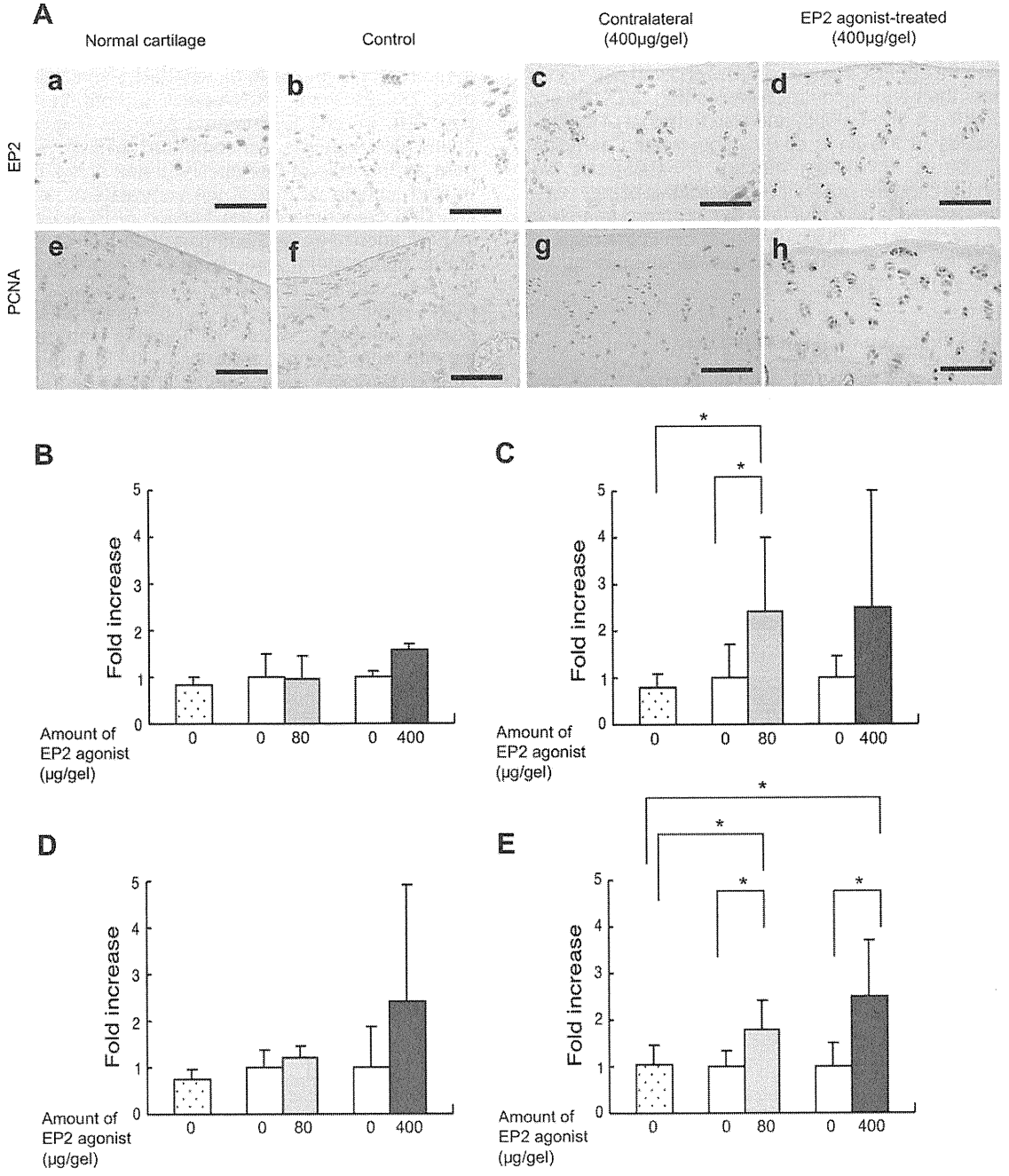

Fig. 3. EP2 agonist promotes proliferation of EP2-positive cells. A: Expression of EP2 and PCNA in normal and regenerated cartilage of chondral defect model. Specimens were prepared from a normal femur without any treatment (a and e), a control sample (b and f), a contralateral sample (c and g), and an EP2 agonist-treated (400 μg/gel) sample (d and h) at 12 weeks after the operation. Immunohistochemical staining was performed with anti-EP2 Ab (a–d) or anti-PCNA Ab (e–h). Bar = 100 μm. B–E: Quantitative analysis of PCNA-positive cells. Cells positive for PCNA staining were counted under the microscope, and a labeling index was calculated for each sample. The relative increase in PCNA-positive cells is expressed as the ratio of the labeling index of the EP2 agonist-treated sample (shaded bars) vs that of the contralateral sample (open bars). The labeling index of control sample relative to those of contralateral sample was indicated in dotted boxes. Samples were prepared from the chondral defect model at 4 weeks (B), chondral defect model at 12 weeks (C), osteochondral defect model at 4 weeks (D), and osteochondral defect model for 12 weeks (E), $^*P < 0.05$.

after the operation, the osteochondral defects were filled with regenerated tissue in all cases, but there was a significant difference in histological scale between EP2 agonist-treated and control samples [Fig. 2(D): 80 μg, $P = 0.005$; 400 μg, $P = 0.0003$]. As in the chondral defect model, the difference was not significant between EP2 agonist-treated than contralateral samples [Fig. 2(D): 80 μg, $P = 0.07$; 400 μg, $P = 0.21$].

At 12 weeks after operation, the effect of EP2 agonist treatment was much evident. The osteochondral defect of EP2 agonist-treated samples was filled with Safranin-O and type II collagen-positive tissues [Fig. 2(C)], and the grading scale of EP2 agonist-treated samples showed and significantly better than that of control samples [Fig. 2(D): 80 μg, $P = 0.002$; 400 μg, $P = 0.0003$] and also than that of contralateral samples in the case of 80 μg/gel-treated samples [Fig. 2(D): 80 μg, $P = 0.006$; 400 μg, $P = 0.05$]. As we observed in the chondral defect model, the scale of contralateral samples tended to be better than that of control samples, and the difference was statistically significant in the case of contralateral sample in 400 μg/gel-treated animals at 12 weeks [Fig. 2(D), $P = 0.005$].

EP2 AGONIST STIMULATED THE PROLIFERATION OF EP2-POSITIVE CELLS

In normal cartilage, almost all cells were EP2-positive as we previously demonstrated in mice and human articular cartilage[11] [Fig. 3(A, a)]. Almost all cells in regenerated tissues of chondral defect model at 12 weeks after operation expressed the EP2 receptor in control [Fig. 3(A, b)], contralateral [Fig. 3(A, c)] and EP2-treated samples (400 μg/gel) [Fig. 3(A, d)]. Identical results were observed in samples harvested at 12 weeks after operation (data not shown), suggesting that the cartilage regeneration was conducted mainly by EP2-positive cells. To evaluate the proliferating ability of these EP2-positive cells, same specimens were used for PCNA staining [Fig. 3(A, e–h)]. Almost no cells were PCNA-positive in normal cartilage [Fig. 3(A, e)] and control sample [Fig. 3(A, f)], whereas some cells in regenerated tissues were PCNA-positive both in contralateral [Fig. 3(A, g)] and EP2-treated samples [Fig. 3(A, h)]. For quantitative analysis, we compared relative PCNA-positive cells as the ratio of the labeling index of the EP2 agonist-treated sample vs that of the contralateral sample. In the chondral defect model, the fraction of PCNA-positive cells in EP2 agonist-treated samples was almost the same as that in contralateral samples at 4 weeks [Fig. 3(B): 80 μg, $P = 0.47$; 400 μg, $P = 0.19$]. At 12 weeks, the fraction of PCNA-positive cells seemed to be higher in EP2 agonist-treated samples than in contralateral samples, although the difference was not convincing due to the wide variation among samples [Fig. 3(C): 80 μg, $P = 0.04$; 400 μg, $P = 0.12$]. In the osteochondral defect model, the fraction of PCNA-positive cells in EP2-treated samples was not

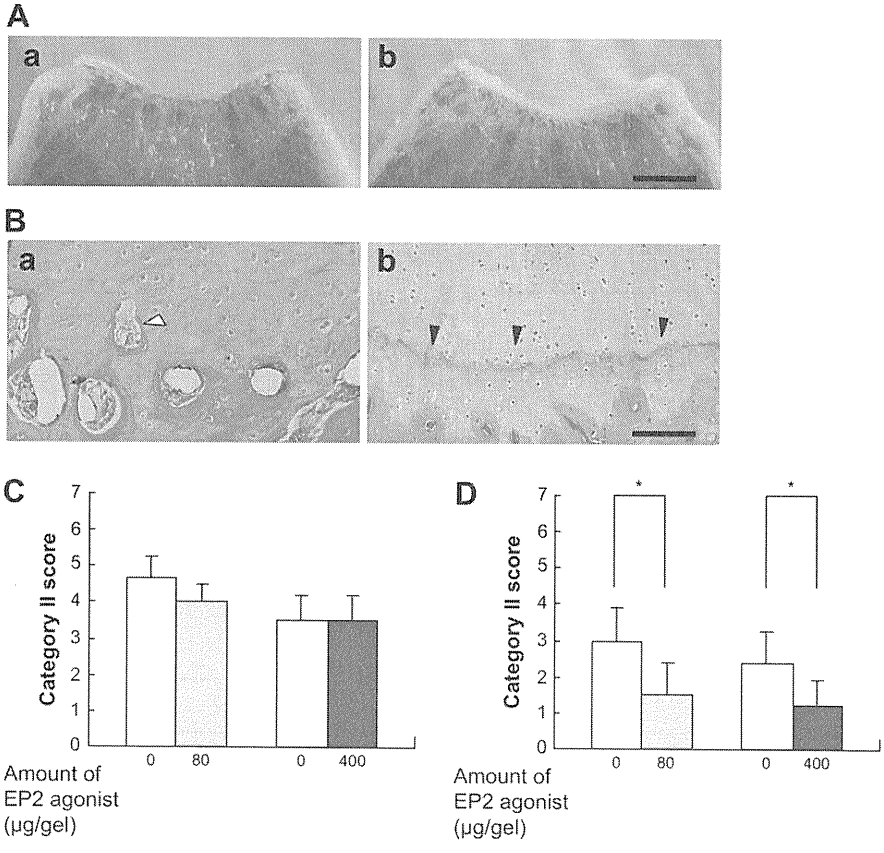

Fig. 4. Effect of EP2 agonist on remodeling of the deep layer zone in chondral defect model. A: Macroscopic view of specimens from contralateral sample (a) and EP2 agonist-treated (400 μg/gel) sample (b) of chondral defect model at 12 weeks after the operation. Bar = 4.0 mm. B: Microscopic view of the osteochondral boundary in the specimens presented in (A). (a) Contralateral sample, (b) EP2 agonist-treated (400 μg/gel) sample. Note that there was no clear boundary, and vascular invasion into articular chondrocytes (white arrowhead) was observed in (a), whereas a clear tidemark (black arrowhead) was formed in (b). Magnification 40×. Bar = 100 μm. C and D: Quantitative evaluation of the osteochondral boundary. The boundary formed between articular cartilage and subchondral bone was evaluated by category II scale of the modified Wakitani scale (0–7, 7 is worse). Samples were prepared from the chondral defect model at 4 weeks (C) and at 12 weeks (D), $^*P < 0.05$.

different from those in contralateral samples at 4 weeks [Fig. 3(D): 80 μg, $P = 0.31$; 400 μg, $P = 0.46$], but significantly higher at 12 weeks [Fig. 3(E): 80 μg, $P = 0.02$; 400 μg, $P = 0.02$]. In all settings, the labeling index of control samples showed no difference from those of contralateral samples [Fig. 3(B): $P = 0.47$; Fig. 3(C): $P = 0.31$; Fig. 3(D): $P = 0.1$; Fig. 3(E): $P = 0.43$].

EP2 AGONIST REPAIRED THE OSTEOCHONDRAL BOUNDARY

Reconstruction of the physiological boundary between articular cartilage and underlying bone tissue is important to maintain the mechanical and biological properties of articular cartilage. Macroscopical examination of EP2 agonist-treated (400 μg/gel) samples in chondral defect model at 12 weeks after operation showed a clear boundary between articular cartilage and subchondral bone [Fig. 4(A, b)]. Microscopical examination demonstrated the reconstruction of the tidemark [Fig. 4(B, b)]. These findings were not observed in contralateral samples. The boundary was not clear in macroscopical examination [Fig. 4(A, a)], and microscopical examination also showed no boundary with some vascular structures in the cartilaginous portion [Fig. 4(B, a)]. The difference was quantitatively evaluated using the category II scale of the modified Wakitani scale. There was no significant difference between EP2 agonist-treated and contralateral samples at 4 weeks [Fig. 4(C)], but the scale was significantly lower in the former than the latter at 12 weeks after operation [Fig. 4(D): 80 μg, $P = 0.03$; 400 μg, $P = 0.04$].

Similar findings were obtained in the osteochondral defect model (Fig. 5). EP2 agonist-treated (400 μg/gel) samples in osteochondral defect model at 12 weeks after operation the showed a clear boundary between articular cartilage and subchondral bone by macroscopical and microscopical examinations [Fig. 5(A, b and B, b)], which were not observed in contralateral samples [Fig. 5(A, a and B, a)]. Quantitative evaluation demonstrated that the boundary was much better formed in 400 μg/gel-, but not 80 μg/gel-treated samples than in contralateral samples at 12 weeks after operation [Fig. 5(D): 80 μg, $P = 0.07$; 400 μg, $P = 0.009$]. This difference was not observed in samples at 4 weeks [Fig. 5(C)]. These results suggest that the EP2 agonist improved the environment surrounding cartilage.

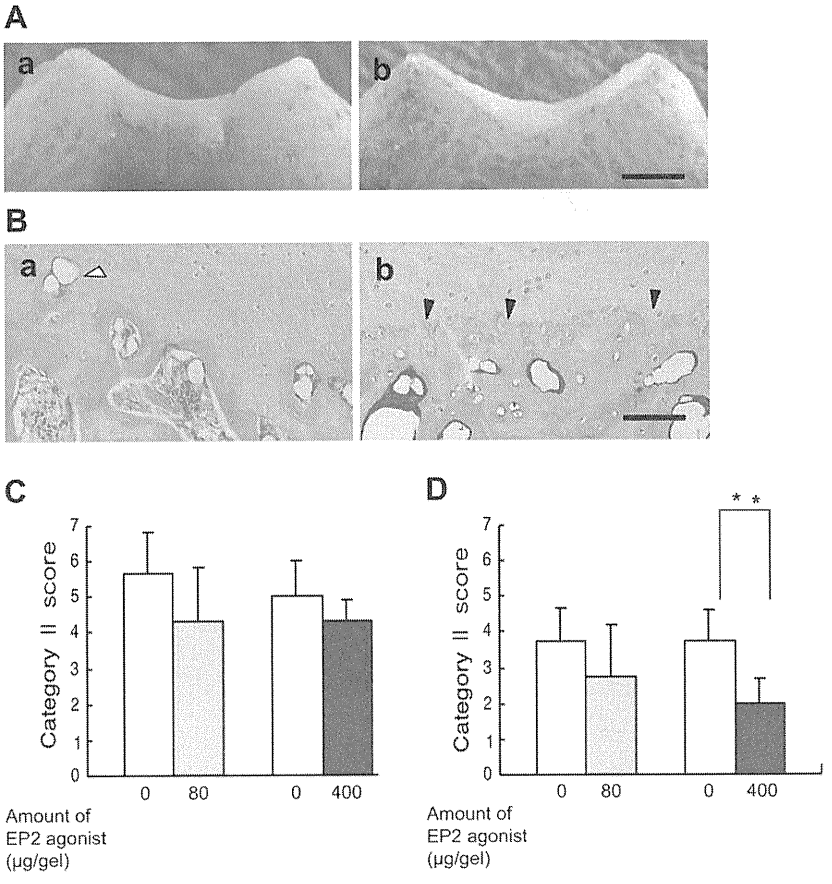

Fig. 5. Effect of EP2 agonist on remodeling of the deep layer zone in osteochondral defect model. A: Macroscopic view of specimens from contralateral sample (a) and EP2 agonist-treated (400 μg/gel) sample (b) of osteochondral defect model at 12 weeks after the operation. Bar = 4.0 mm. B: Microscopic view of the osteochondral boundary in the specimens presented in (A). (a) Contralateral sample (b) EP2 agonist (400 μg/gel)-treated sample. Note that there was no clear boundary, and vascular invasion into articular chondrocytes (white arrowhead) was observed in (a), whereas a clear tidemark (black arrowhead) was formed in (b). Magnification 40×. Bar = 100 μm. C and D: Quantitative evaluation of the osteochondral boundary. The boundary formed between articular cartilage and subchondral bone was evaluated by category II scale of the modified Wakitani scale (0–7, 7 is worse). Samples were prepared from the chondral defect model at 4 weeks (C) and at 12 weeks (D), $^{**}P < 0.01$.